Aus der Klinik für
Allgemein, Viszeral- und Transplantationschirurgie der Universität München
Direktor: Prof. Dr. med. Jens Werner

Der Effekt innovativer Immunsuppressiva auf die akute Transplantatabstoßung im allogenen Nierentransplantations-Modell in der Maus

Dissertation
zum Erwerb des Doktorgrades der Medizin
an der Medizinischen Fakultät
der Ludwig-Maximilians-Universität zu München

vorgelegt von

Benjamin Michael Ehle

aus Kaufbeuren

2024

Mit Genehmigung der Medizinischen Fakultät
der Universität München

Berichterstatter:	Prof. Dr. Joachim Andrassy
Mitberichterstatter:	Prof. Dr. Jürgen E. Scherbich
	Prof. Dr. Thomas Sitter
Dekan:	Prof. Dr. med. Thomas Gudermann
Tag der mündlichen Prüfung:	04.07.2024

Affidavit

Eidesstattliche Versicherung

Ehle, Benjamin Michael

Name, Vorname

Ich erkläre hiermit an Eides statt, dass ich die vorliegende Dissertation mit dem Titel:

Der Effekt innovativer Immunsuppressiva auf die akute Transplantatabstoßung im allogenen Nierentransplantations-Modell in der Maus

selbständig verfasst, mich außer der angegebenen keiner weiteren Hilfsmittel bedient und alle Erkenntnisse, die aus dem Schrifttum ganz oder annähernd übernommen sind, als solche kenntlich gemacht und nach ihrer Herkunft unter Bezeichnung der Fundstelle einzeln nachgewiesen habe.

Ich erkläre des Weiteren, dass die hier vorgelegte Dissertation nicht in gleicher oder in ähnlicher Form bei einer anderen Stelle zur Erlangung eines akademischen Grades eingereicht wurde.

München, 22.07.2024

Ort, Datum

Ehle Benjamin Michael

Unterschrift Doktorand

Inhaltsverzeichnis

Abkürzungsverzeichnis

Cat-S	Cathepsin S
CCR2	C-C chemokine receptor type 2
DCE-MRT	Dynamic contrast enhanced-MRT
DW-MRT	Diffusion weighted-MRT
i.p.	intraperitoneal
MCP-1	Monocyte chemoattractant protein 1
MHC	Major histocompatibility complex
PAR-2	Protease activated receptor 2
RT-PCR	Real time-Polymerase chain reaction
s.c.	subkutan
3T MRT	3 Tesla Magnetresonanztomographie

Publikationsliste

Lung Resections for Elderly Patients with Lung Metastases: A Comparative Study of the Postoperative Complications and Overall Survival

Hassan M, **Ehle B**, Passlick B, Grapatsas K. Curr Oncol 2022;29:4511-4521.

Outcome of Repeated Resection of Pulmonary Metastases for Renal Cell Cancer

Hassan M, **Ehle B**, Le UT, Titze L, Passlick B, Grapatsas K. Thorac Cardiovasc Surg 2022; Epub 2022 Aug 20.

Can Chest Ultrasound Replace Chest X-ray in Thoracic Surgery?

Grapatsas K, Leivaditis V, **Ehle B**, Papaporfyriou A. Thomography 2022;8:2082-2092.

Lung Metastatectomy: Can Laser-Assisted Surgery Make a Difference?

Grapatsas K, Papaporfyriou A, Leivaditis V, **Ehle B**, Galanis M. Curr Oncol 2022;29:6968-6981.

Should cardiovascular comorbidities be a contraindication for pulmonary metastasectomy?

Grapatsas K, Hassan M, Semmelmann A, **Ehle B**, Passlick B, Schmid S, Le UT. J Thorac Dis 2022;14:4266-4275.

1. Beitrag zu den Publikationen I und II

Die Durchführung der Spender- und Empfängeroperation der orthothopen Nierentransplantation in der Maus unter einem Operationsmikroskop wie unter 2.4 detailliert beschrieben, erfolgte für die erste Publikation zu großen Teilen und für die zweite Publikation komplett eigenständig.

Dies beinhaltete ebenfalls die Narkoseführung, die postoperative analgetische Therapie, die Applikation von Medikamenten, die Überwachung nach der Operation anhand eines Bewertungsbogen für die postoperative Belastung sowie die Organentnahme zur weiteren Analyse am Ende des Beobachtungszeitraums.

Zusätzlich wurde in eigenständiger Arbeit ein neuartiges Verfahren der Ureteranastomose, wie von Han et. al. beschrieben, mittels Durchzugsmethode etabliert. Die Ureteranastomose ist die Achillesferse der Nierentransplantation in der Maus, mit hohen Insuffizienzraten mit einem letalen Ausgang. Durch diese technische Weiterentwicklung der Ureteranastome kam es zu keiner einzigen Insuffizienz.

Für beide Projekte habe ich zudem bei der histopathologischen Aufarbeitung der Präparate wie auch bei der Durchführung der RT-PCR mitgeholfen.

Ferner war ich in wöchentlichen Labormeetings mit meinen Arbeitsgruppenleitern in einem konstruktiven Dialog für die jeweilige Projektausrichtung.

Auch war ich bei der Erstellung beider Manuskripte beteiligt.

2. Einleitung

2.1 Aktueller Stand der Nierentransplantation

Die Nierentransplantation ist heute die etablierte Standardtherapie der chronisch terminalen Niereninsuffizienz und kann als präemptive Transplantation einer Niere bei noch nicht terminalen Nierenversagen erfolgen mit allein in Deutschland im Jahre 2021 insgesamt 1992 durchgeführten Nierenverpflanzungen [1].

Meilensteine hierfür waren die Entwicklung moderner Naht- und Anastomosentechniken durch Alexis Carrel, neue und bahnbrechende Erkenntnisse auf dem Gebiet der Transplantationsimmunologie sowie die Entdeckung immunsuppressiver Medikamente, die den initial experimentellen Charakter der Nierentransplantation, 1954 durch J. Murray erstmals erfolgreich durchgeführt, zu einem chirurgischen Standardeingriff haben werden lassen [2, 3, 4].

Hierbei zeigt sich eine deutliche Überlegenheit der Nierentransplantation gegenüber den Dialyseverfahren im Langzeitverlauf in Bezug auf Kosten, Lebensqualität und Langzeitüberleben [5].

Trotz der Erfolgsgeschichte der Nierentransplantation mit heutzutage erzielten 1 Jahres Transplantatüberleben von bis zu 90% blieben gleichwertige Erfolge für das Langzeittransplantatüberleben leider aus [6, 7].

Aggraviert wird diese Situation durch den Rückgang an Organspenden auf der einen Seite und dem stetig steigenden Bedarf an Spenderorganen auf der anderen Seite [8].

Die Ätiologie der chronischen Allotransplantatschädigung ist multifaktoriell mit sowohl immunologischen als auch nicht-immunologischen Ursachen [9, 10, 11].

Die gemeinsame pathophysiologische Endstrecke stellt die Transplantatvaskulopathie mit sukzessiver Parenchymfibrose und Funktionsverlust dar [12, 13].

Hauptursachen hierfür sind rezidivierende Episoden akuter Transplantabstoßungen sowie das nephrotoxische Nebenwirkungsprofil aktueller immunsuppressiver Therapieregime [14, 15].

Der übergeordnete Gesamtzusammenhang der beiden Veröffentlichungen, die dieser kumulativen Dissertation zu Grunde liegen, ist die Erforschung des renoprotektiven Effektes innovativer Immunsuppressiva auf die akute Allotransplantatabstoßung im Modell der murinen Nierentransplantation.

2.2 Hemmung der MCP-1-/CCR2-Achse

In der ersten Veröffentlichung “Multiparametric Functional MRI: A Tool to Uncover Subtle Changes following Allogenic Renal Transplantation” wurde der Einfluss der Chemokinhemmung der MCP-1-/CCR2-Achse auf die immunologischen Vorgänge der Allotransplantatabstoßung im murinen Nierentransplantationsmodell untersucht.

Chemokine sind Signalproteine, die eine Schlüsselrolle in der Migration (Chemotaxis) und Aktivierung von Immunzellen spielen und ihre Wirkung durch Bindung an Chemokinrezeptoren entfalten [16].

Bei der Transplantation solider Organe konnte gezeigt werden, dass Chemokine am Prozess des Ischämie-Reperfusionsschaden sowie der akuten und chronischen Transplantatabstoßung wesentlich beteiligt sind [17].

MCP-1 ist das Chemokin mit der stärksten chemotaktischen Wirkung und sein Rezeptor, CCR2, zeigt eine starke Expression auf Monozyten und aktivierten T-Zellen [18, 19].

In anderen Arbeiten wurde bereits demonstriert, dass die Hemmung der MCP-1-/CCR2-Achse die Allotransplantatabstoßung im Modell der murinen Lungentransplantation und Inselzelltransplantation schwächt [20, 21].

Die pharmakologische Hemmung der MCP-1/CCR2-Achse erfolgte in unseren Versuchsreihen durch das Spiegelmer mNOX-E36 der Firma Noxxon, welches bereits seine Effektivität in einem vorangegangenen Projekt im Modell der heterotopen Herztransplantation in der Maus unter Beweis gestellt hat [22].

Spiegelmere sind stereochemische Spiegelbilder natürlicher Oligonukleotide, die entsprechende pharmakologische Zielstrukturen ähnlich wie ein Antikörper binden können und aufgrund ihres spiegelbildlichen Aufbaus nicht immunogen sind sowie eine erhöhte Biostabilität aufweisen, da sie von den natürlich vorkommenden Nukleasen nicht erkannt werden können [23, 24].

Im Versuchsaufbau gab es insgesamt 5 verschiedene Gruppen, mit einer jeweiligen Gruppengröße von n=5 Mäusen, die alle männlich in einem Alter zwischen 7-14 Wochen waren. Die Empfängertiere waren allesamt C57Bl/6 Mäuse. In der Kontrollgruppe wurden syngene Nierentransplantationen mit C57Bl/6 Mäusen als Spendertiere durchgeführt. Im weiteren allogenen Transplantationssetting dienten Balb/c Mäuse als Spendertiere. Hier gab es eine zusätzliche Kontrollgruppe mit dem funktionsunfähigen Spiegelmer revmNOX-E36 (15,5 mg/kgKG/Tag). Die Therapiegruppe erhielt das funktionsfähige Spiegelmer mNOX-E36 (15,5 mg/kgKG/Tag). Um einen möglichen additiven Effekt der Zytokinhemmung mit mNOX-E36 in Kombination mit dem etablierten Immunsuppressivum Ciclosporin

A zu detektieren, wurde eine weitere Gruppe mit einer Kombinationstherapie aus mNOX-E36 und Ciclosporin A (15,5 mg/kgKG/Tag und 10,0 mg/kgKG/Tag) sowie eine weitere entsprechende Kontrollgruppe mit Ciclosporin A Monotherapie (10,0 mg/kgKG/Tag) transplantiert. Die Medikamentenapplikation erfolgte durch i.p.-Injektion.

Zusätzlich zur regulären Auswertung, welche unter dem Punkt 2.5 beschrieben wird, erfolgte in dieser Publikation exklusiv am 10. postoperativen Tag die Durchführung einer Diffusion-weighted- und Dynamic-contrast-enhanced MRT-Untersuchung als nicht-invasives funktionelles bildgebendes Verfahren zur Detektion der Prozesse der Allotransplantatabstoßung in Korrelation mit den Ergebnissen der weiteren histologischen Aufarbeitung [25, 26, 27].

Der Hintergrund hierfür ist die Tatsache, dass auch heute noch akute Nierenallotransplantatabstoßungen schwer und zeitverzögert detektiert werden und hierfür eine invasive Gewebebiopsie nötig ist, die mit möglichen schweren Komplikationen, wie einer Infektion oder Blutung, vergesellschaftet sein können [28, 29].

Eine nicht-invasive Methode ohne Strahlenbelastung zur Detektion einer Allotransplantatabstoßung könnte hierfür in Zukunft mittels MRT-Untersuchung erfolgen [30].

2.3 Hemmung der Cathepsin S-/PAR-2-Achse

In der zweiten Veröffentlichung „Cathepsin S and Protease-Activated Receptor-2 Drive Alloimmunity and Immune Regulation in Kidney Allograft Rejection“ wurde der Einfluss der Hemmung der Cathepsin S/ PAR2-Achse auf die immunologischen Vorgänge der Allotransplantatabstoßung im murinen Nierentransplantationsmodell untersucht.

Cathepsin S ist eine Cysteinprotease mit intra- und extrazellulären Angriffspunkten [31, 32, 33].

Intrazellulär ist Cat-S nicht redundant an der Beladung von MHC-Klasse-II Molekülen antigenpräsentierender Zellen mit (allo-) antigenen Peptid beteiligt [34].

Ein zentraler Mechanismus der Alloimmunität ist die Präsentation von Alloantigenen mittels MHC-Klasse-II-Moleküle durch antigenpräsentierende Zellen sowohl des Empfängers als auch des Spenders gegenüber T-Lymphozyten des Empfängers, der sogenannten indirekten bzw. direkten Alloantigenerkennung [35, 36, 37].

Zur Verhinderung einer vorzeitigen oder falschen Beladung der Antigenbindungsstelle der im endoplasmatischen Retikulum heranreifenden MHC-Klasse-II-Moleküle ist diese zunächst mit der sogenannten invariant chain Li blockiert. Es erfolgt die sukzessive enzymatisch Stutzung der invariant chain Li, bis zuletzt der Austausch des kleinsten blockierenden Fragments, CLIP, gegen das antigene Peptid erfolgt. Dieser letzte Schritt ist abhängig von Cat-S. Die pharmakologische Inhibition von Cat-S verhindert die Entstehung von CLIP, mit konsekutivem Verbleib der invariant chain Li in der Antigenbindungsgrube des MHC-Klasse-II-Molekül. Die Beladung des MHC-Klasse II Molekül mit (allo-)antigenem Peptid bleibt somit aus, was konsekutiv zu einer Hemmung der (Allo-)Antigen-Präsentation führt [38, 39, 40, 41].

Extrazellulär ist Cat-S direkt und indirekt an makro- und mikroangiopathischen Gefäßschädigung beteiligt [42, 43].

Die extrazelluläre Sekretion von Cat-S erfolgt durch Monozyten/Makrophagen, Neutrophile und Endothelzellen. Cat-S besitzt die Fähigkeit direkt elastische Fasern zu spalten und spielt hierdurch eine Rolle im Entstehungsmechanismus von Gefäßaneurysmen und fördert die Progression der arteriosklerotischen Degeneration von Gefäßwänden [44].

Eine indirekte Gefäßschädigung durch Cat-S wird durch PAR-2, einem G-Protein gekoppelten Rezeptor auf Gefäßendothelzellen, vermittelt. Dieser wird durch Cat-S aktiviert und die hierdurch eingeleiteten Signaltransduktionswege führen zu einer nachfolgenden Endotheldysfunktion [45, 46, 47].

Arbeitshypothese:

Die Hemmung der Cat-S/PAR-2-Signalkaskade bewirkt einen positiven Effekt auf den Prozess der murinen Nierenallotransplantatabstoßung.

Orthotope Nierentransplantationen in der Maus wurden in nachfolgenden Spender-Empfänger-Konstellationen in zwei verschiedenen Versuchsreihen A und B aufgrund der jeweils unterschiedlichen Therapieregime durchgeführt.

Die Versuchsreihe A bestand aus einer syngenen Kontrollgruppe und einer allogenen Kontrollgruppe jeweils ohne Therapie sowie einer allogenen Therapiegruppe. Die Empfängertiere waren allesamt C57BL/6 Mäuse. Die Spendertiere der syngenen Gruppe waren C57BL/6 Mäuse und die der allogenen Gruppen Balb/c Mäuse. Die jeweilige Gruppengröße umfasste n=10 Tiere. Die Therapie bestand in der zweimal täglichen gewichtsadaptierten oralen Verabreichung des Cat-S Inhibitor RO5461111 beginnend einen Tag vor der Nierentransplantation über den gesamten Beobachtungszeitraum.

In der Versuchsreihe B wurde ebenfalls eine syngene und eine allogene Kontrollgruppe ohne Therapie sowie eine allogene Therapiegruppe gebildet. Die „Therapie“ bestand hier jedoch in der Transplantation von Spendernieren aus PAR-2-Knockout-Mäusen um zu zeigen, dass auch die alleinige Hemmung der PAR-2 abhängigen Signaltransduktionswege einen positiven Einfluss auf die Allotransplantatabstoßung zeigt. Da die verwendeten Knockout-Mäuse in Bezug auf ihre Genetik einen C57BL/6 Hintergrund aufweisen, musste im Vergleich zur Versuchsreihe A eine vertauschte Spender-Empfänger-Konstellation gewählt werden, mit Balb/c Mäusen als Empfängertiere in allen Gruppen sowie als syngene Spendertiere und die C57BL/6 Mäuse als Spendertiere in der allogenen Kontrollgruppe ohne Therapie sowie die C57BL/6.PAR2 -/- Mäuse als Spendertiere in der Therapiegruppe.

Der Beobachtungszeitraum in beiden Versuchsreihen erstreckte sich jeweils bis zum 10. postoperativen Tag und es erfolgte keine weitere immunsuppressive Therapie außer der oben genannten.

2.4 Modell der murinen Nierentransplantation

Alle Versuche waren durch den Tierversuchsantrag GZ 55.2-1-54-2532-80-2015 der Regierung von Oberbayern angezeigt und durch diese bewilligt worden.

Orthothope Nierentransplantationen in der Maus, erstbeschrieben von Skośkiewicz et al. wurden mit leichten Modifikationen nach Russel et al. sowie Wang und Han et al. durchgeführt [48, 49, 50, 51].

Die beiden Eigennieren des Empfängertieres wurden belassen, sodass die Mäuse nicht von der Funktion der transplantierten Niere abhängig waren. Daher erfolgte auch keine Bestimmung von Nierenfunktionsparametern wie Serumkreatinin oder Harnstoff.

Nach dem 10. postoperativen Tag erfolgte die Entnahme der Nieren zur weiteren Analyse.

2.5 Auswertung

Die Aufarbeitung der Effekte dieser neuartigen immunsuppressiven Medikation auf den Prozess der akuten murinen Nierenallotransplantatabstoßung wurde in beiden Arbeiten anhand der Histopathologie, der Immunhistochemie und der RT-PCR durchgeführt.

Die Begutachtung der Histopathologie erfolgte anhand der 4 Kriterien Glomerulitis, interstitielle Inflammation, intimale Arteritis und Tubulitis, semiquantitativ abgebildet in einem 4 Punkte-Score (0-3) in Anlehnung an die Banff-Kriterien [52].

In der Immunhistochemie erfolgte die Färbung für den Monozyten/Makrophagen-Oberflächen-Marker F4/80+, da diese Immunzellen bei der akuten Nierenallotransplantatabstoßung prädominierend sind [53].

In der RT-PCR erfolgte die Bestimmung der Expression verschiedener, für die akute Allotransplantatabstoßung relevanter Zytokine, wie unter anderem Interferon-gamma und TNF-alpha [54].

3. Zusammenfassung

Ziel dieser Doktorarbeit war die Erforschung des immunsuppressiven und organoprotektiven Effekts innovativer Pharmaka.

In der ersten Veröffentlichung

“Multiparametric Functional MRI: A Tool to Uncover Subtle Changes following Allogeneic Renal Transplantation”

wurde die Chemokinhemmung der MCP-1/CCR2-Signalkaskade durch das Spiegelmer mNOX-E36 auf die immunologischen Vorgänge bei der Allotransplantatabstoßung nach muriner Nierentransplantation untersucht. Die Spiegelmer-Hemmung zeigte einen synergistischen Effekt in Kombination mit Cyclosporin A im Vergleich zur Cyclosporin A Monotherapie.

Hierfür wurden orthotope Nierentransplantationen in der Maus in insgesamt 5 verschiedenen Gruppen durchgeführt, wobei die jeweilige Gruppengröße n=5 Mäuse umfasste und alle Empfängertiere C57BL/6 Mäuse waren.

Je eine Therapiegruppe erhielt das nicht funktionelle Spiegelmer revmNOX-E36, eine das funktionstüchtige Spiegelmer mNOX-E36, eine Cyclosporin A als Monotherapie und eine die Kombinationstherapie mit mNOX-E36 und Cyclosporin A.

Die Medikamente wurden jeden Tag i.p. gewichtsadaptiert über den kompletten Beobachtungszeitraum von 10 Tagen appliziert.

Der Read-out erfolgte über die Histopathologie der Nierentransplantate mit Orientierung an den Banff-Score Kriterien Glomerulitis, interstitielle Inflammation, Intima Arteriitis und Tubulitis, der immunhistochemischen Quantifizierung der Transplantatinfiltration mit Monozyten und der Bestimmung der mRNA-Expressionslevel an IFN-gamma, TNF-alpha, und B-cell activating factor durch RT-PCR in den Transplantaten.

Zusätzlich wurde vor der Organentnahme mittels 3T-MRT eine funktionelle Bildgebung (DW-/DCE-MRT) durchgeführt, um den nichtinvasiven Nachweis in vivo in Bezug auf die Erkennung der Transplantatschädigung und des Effektes der immunsuppressiven Therapie in Korrelation zu den oben gewonnenen Daten zu erbringen.

Die Monotherapie mit mNOX-E36 ging mit einer signifikanten Reduktion der Monozyteninfiltration und einer verminderten Expression an proinflammatorischen Zytokinen in den Nierenallotransplantaten einher, wohingegen sich ungeachtet dessen keine Verbesserung im histologischen Bild zeigte.

Ein additiver Effekt der pharmakologischen Hemmung der MCP-1/CCR2-Achse konnte für die Kombinationstherapie mit Cyclosporin A in fast allen Experimenten festgestellt werden sowie die Möglichkeit, mittels funktioneller MRT-Bildgebung Therapieeffekte der Immunsuppression und der Transplantatabstoßung nichtinvasiv zu detektieren.

In der zweiten Veröffentlichung

„Cathepsin S and Protease-Activated Receptor-2 Drive Alloimmunity and Immune Regulation in Kidney Allograft Rejection“

sollte der Nachweis erbracht werden, dass eine Hemmung der Cat-S/PAR-2-Achse einen organoprotektiven Einfluss auf die immunologischen Prozesse der akuten murinen Nierenallotransplantatabstoßung zeigt.

Orthotope Nierentransplantationen in der Maus wurden in nachfolgenden Spender-Empfänger-Konstellationen in den zwei verschiedenen Versuchsreihen A und B aufgrund der jeweils unterschiedlichen Therapieregime durchgeführt.

Die Versuchsreihe A bestand aus einer syngenen Kontrollgruppe und einer allogenen Kontrollgruppe jeweils ohne Therapie sowie einer allogenen Therapiegruppe. Die Empfängertiere waren allesamt C57BL/6 Mäuse. Die Spendertiere der syngenen Gruppe waren C57BL/6 Mäuse und die der allogenen Gruppen Balb/c Mäuse. Die jeweilige Gruppengröße umfasste n=10 Tiere. Die Therapie bestand in der zweimal täglichen gewichtsadaptierten oralen Verabreichung des Cat-S Inhibitor RO5461111 beginnend einen Tag vor der Nierentransplantation über den gesamten Beobachtungszeitraum.

In der Versuchsreihe B wurde ebenfalls eine syngene und eine allogene Kontrollgruppe ohne Therapie sowie eine allogene Therapiegruppe gebildet. Die „Therapie“ bestand hier jedoch in der Transplantation von Spendernieren aus PAR-2-Knockout-Mäusen um zu zeigen, dass auch die alleinige Hemmung der PAR-2 abhängigen Signaltransduktionswege einen positiven Einfluss auf die Allotransplantatabstoßung zeigt.

Der Beobachtungszeitraum in beiden Versuchsreihen erstreckte sich jeweils bis zum 10. postoperativen Tag und es erfolgte keine weitere immunsuppressive Therapie außer der oben genannten.

Der Read-out erfolgte anhand der histopathologischen Auswertung der Nierentransplantate mit Orientierung an den Banff-Score Kriterien wie Glomerulitis, Intima Arteriitis, interstitielle Inflammation und Tubulitis sowie mittels $CD8^+$T-Zell-

Färbung in der Immunhistochemie und durch die Bestimmung der mRNA-Expressionslevel von in der Transplantationsmedizin relevanten Chemokinen und Zytokinen in der RT-PCR.

Zusammenfassend lässt sich grundlegend festhalten, dass im Rahmen der Abstoßungsreaktion erhöhte Expressionslevel an Cat-S bzw. PAR-2 in murinen Nierenallotransplantaten vorlagen.

Zusätzlich konnte gezeigt werden, dass durch die pharmakologische Hemmung des Cat-S durch RO5461111 als auch durch die alleinige Hemmung der PAR-2 abhängigen Signaltransduktionswege mittels PAR2 -/- Spendernieren als „Therapie“ eine signifikante Abschwächung der murinen Nierenallotransplantatabstoßung bewirkt, nachweislich durch eine Reduktion der histopathologischen Allotransplantatschädigung, durch eine Reduktion der $CD8^+$-T-Zellinfiltration im Allotransplantat und durch eine Reduktion der Expressionslevel an transplantationsrelevanten Chemokinen und Zytokinen im Allotransplantat.

4. Abstract

The objective of this doctoral thesis was the investigation of the immunosuppressive and organ protective effect of innovative pharmaceuticals.

The first publication

“Multiparametric Functional MRI: A Tool to Uncover Subtle Changes following Allogeneic Renal Transplantation”

investigated the chemokine inhibition of the MCP-1/CCR2-axis through the spieglmer mNOX-E36 in the setting of murine kidney allotransplantation.

Murine orthotopic kidney transplantations were performed in five different groups. Each group size consists of n=5 mice. All recipients were C57BL/6 mice.

One therapy group received the non-functioning spiegelmer revmNOX-E36, one the functioning spiegelmer mNOX-E36, one ciclosporine A monotherapy and one the combination therapy of mNOX-E36 and ciclosporin A.

The drugs have been applicated weight-adapted every day i.p. for the whole observation period of 10 days.

The read-out was performed by histopathology with an orientation according to the Banff-score criteria glomerulitis, interstitial inflammation, intimal arteritis and tubulitis, the immunhistochemical quantification of transplant infiltration by monocytes and the determination of mRNA-expression level of IFN-gamma, TNF-alpha, and B-cell activating factor by RT-PCR.

In addition a functional imaging (DW-/DCE-MRT) with a 3T-MRT was carried out before the organ removal to show non-invasively in vivo the damage of the allotransplant and the immunosuppressive effect in correlation to the acquired data.

Monotherapy with mNOX-E36 showed a significant reduction of monocyte infiltration and a reduced expression of proinflammatory cytokines in kidney allotransplants, whereas no improvement of the histology has been detected.

An additive effect of the pharmaceutical inhibition of the MCP-1/CCR2-axis was demonstrated for the combination therapy with ciclosporin A in almost all experiments as well as the possibility of determining therapeutic effects of the immunosuppression and the transplant rejection non-invasively by functional MRT imaging.

In the second publication

„Cathepsin S and Protease-Activated Receptor-2 Drive Alloimmunity and Immune Regulation in Kidney Allograft Rejection"

we wanted to establish proof of the organ protective effect of Cat-S/PAR-2 axis inhibition on the immunological process of murine kidney allotransplant rejection.

Orthotopic kidney transplantation in the mouse were performed in the following donor and recipient combination in two different series of experiments A and B because of different therapeutic regimes.

In the experimental group A there was a syngenic and allogenic control group without therapy and an allogenic therapy group. All the recipients were C57BL/6 mice.

The donors of the syngenic group were C57BL/6 mice and Balb/c mice in the allogenic group. Each group size included n=10 animals. The therapy consisted of the oral administration of the Cat-S inhibitor RO5461111 twice a day starting one day prior to the kidney transplantation and extended over the whole observation time.

The experimental group B was built up of a syngenic and an allogenic control group without therapy and an allogenic therapy group.

The therapy consisted in the transplantation of PAR-2 knock-out kidneys to show that an exclusive inhibition of PAR-2 dependent signaling pathways has a positive influence on the process of kidney allotransplant rejection.

The observation time in both experimental groups lasted 10 days and there was no additional immunosuppressive therapy.

The read-out was carried out by the histopathology of the kidney transplants with orientation according to the Banff criteria glomerulitis, intimal arteritis, interstitial inflammation and tubulitis as well as CD8+T-cell staining in the immunohistology as well as the detection of mRNA expression levels of relevant cytokines in the RT-PCR.

In summary the acute rejection of murine kidney allotransplants was accompanied by elevated expression levels of Cat-S and PAR-2.

It was further shown that the pharmacological inhibition of Cat-S by RO5461111 as well as the exclusive inhibition of the PAR-2 depending signaling pathways by PAR2 -/- donor kidneys as therapy causes a significant attenuation of the kidney allotransplant rejection.

This was demonstrated by the reduction of the histopathological damage of the transplanted kidneys, the reduction of CD8+ T-cell infiltration of the allotransplants and a reduction of relevant chemokines and cytokines in the setting of kidney allotransplants.

5. Publikation I

Multiparametric Functional MRI: A Tool to Uncover Subtle Changes following Allogeneic Renal Transplantation

Notohamiprodjo M, Kalnins A, Andrassy M, Kolb M, **Ehle B**, Mueller S, Thomas MN, Werner J, Guba M, Nikolaou K, Andrassy J. **(Ko-Autorenschaft)**

Multiparametric Functional MRI: A Tool to Uncover Subtle Changes following Allogeneic Renal

Transplantation.

PLoS One. 2016 Nov 7;11(11):e0165532; IF 3.27

PLOS | ONE

RESEARCH ARTICLE

Multiparametric Functional MRI: A Tool to Uncover Subtle Changes following Allogeneic Renal Transplantation

Mike Notohamiprodjo[1,2]*, Aivars Kalnins[3], Martin Andrassy[4], Manuel Kolb[1,2], Benjamin Ehle[3], Susanna Mueller[5], Michael N. Thomas[3], Jens Werner[3], Markus Guba[3], Konstantin Nikolaou[1], Joachim Andrassy[3]

1 Department of Radiology, University Hospital Tuebingen, Tuebingen, Germany, **2** Department of Clinical Radiology, University Hospitals Munich, Munich, Germany, **3** Department of Surgery, University Hospital Munich, Munich, Germany, **4** Department of Medicine, Rupprecht-Karl's University, Heidelberg, Germany, **5** Department of Pathology, Ludwig-Maximilian's University, Munich, Germany

* Mike.Notohamiprodjo@med.uni-tuebingen.de

OPEN ACCESS

Citation: Notohamiprodjo M, Kalnins A, Andrassy M, Kolb M, Ehle B, Mueller S, et al. (2016) Multiparametric Functional MRI: A Tool to Uncover Subtle Changes following Allogeneic Renal Transplantation. PLoS ONE 11(11): e0165532. doi:10.1371/journal.pone.0165532

Editor: Jaap A. Joles, University Medical Center Utrecht, NETHERLANDS

Received: April 25, 2016

Accepted: October 13, 2016

Published: November 7, 2016

Data Availability Statement: All relevant data are within the paper and its Supporting Information files.

Funding: This work was supported by the Else-Kröner-Fresenius Stiftung (J.A. A 80/09) and by the Förderprogramm für Forschung und Lehre (Antr. 762) of the Ludwig-Maximilians-University Munich. The funders had no role in study design, data collection and analysis, decision to publish, or preparation of the manuscript.

Abstract

Purpose

To investigate multiparametric functional MRI to characterize acute rejection in a murine allogeneic renal transplant model and evaluate the effect of novel therapeutics.

Material and Methods

We performed allogeneic and syngeneic orthotopic transplantations (Balb/c to C57Bl/6 and C57Bl/6 to C57Bl/6). Allogeneic Groups (n = 5) were either treated with the anti-CCL2-Spiegelmer (mNOX-E36) in monotherapy or in combination with low doses of Ciclosporin-A (10mg/kgBW/d) for 10 days. Controls received equivalent doses of a non-functional spiegelmer (revmNOX-E36) or low dose Ciclosporin-A. Diffusion-weighted (DWI) and Dynamic-contrast-enhanced (DCE-) MRI-scans were performed using a clinical 3T-scanner. DWI analysis (b-values from 0–800 s/mm^2) was performed mono- and biexponentially, while DCE-MRI was assessed with deconvolution analysis. Therapy effects were assessed *ex vivo* with histopathology, immunohistochemistry and RT-PCR. Statistical analysis was performed with unpaired t-tests and Spearman´s correlation coefficient.

Results

DWI showed a significant diffusion restriction in allogeneic compared to syngeneic transplants (ADC: 0.63±0.08 vs. 1.29±0.12 mm^2/s*10^3) with decreasing diffusion restriction under therapy. DCE-MRI showed restored organ perfusion under Ciclosporin A alone and combination therapy (Plasma Flow: 43.43±12.49; 38.75±7.53ml/100ml/min) compared to syngeneic controls (51.03±12.49ml/100ml/min). *Ex vivo* analysis showed reduced monocytic infiltrates, attenuated levels of inflammatory cytokines under mNOX-E36 monotherapy with an additive effect of low dose Ciclosporin A. There was a significant ($p<0.05$)

Competing Interests: The authors have declared that no competing interests exist.

negative correlation between ADC and interstitial inflammation (r = -0.73) or macrophage infiltration (r = -0.81) and between organ perfusion and intimal arteritis (r = -0.63).

Conclusion

Multiparametric functional MRI is suited to detect renal allograft rejection in an experimental murine model and allows to characterize effects of immunosuppressive therapy alleviating acute rejection processes in allogeneic transplantation.

Introduction

Kidney transplantation renders formidable short term results with one-year graft survival rates of greater than 90% [1]. However, improvements of long term graft survival have been moderate over the course of the last two decades [2]. This holds true not only for renal but for all other solid organ transplants as well [3]. The immunological barriers, the required immunosuppression with their inherent problems and comorbidity of the recipients are the major factors impairing long-term survival [4].

The assessment of treatment effects of immunosuppressive agents as well as the diagnosis of allograft rejection itself is a major problem in transplant medicine. Changes of respective serum levels in combination with loss of function are indirect signs for ongoing allograft injury/rejection. Though biopsies are routinely performed with a limited risk profile, sampling errors and fatal complications with graft loss or even death can occur [5]. Furthermore, histopathology does not necessarily reveal and reflect pathophysiological and functional changes. Functional Magnetic Resonance Imaging (MRI) may serve as an alternative diagnostic non-invasive method [6] Diffusion weighted Imaging (DWI) allows to assess acute allograft rejection by probing molecular water diffusion. Microcirculation can be assessed by an advanced biexponential analysis of the DWI-data applying the intravoxel incoherent motion (IVIM) model or with dynamic contrast enhanced (DCE-)MRI. In exploratory human studies, these non-invasive imaging methods allowed to distinguish between normally functioning organs, acute allograft rejection and ischemic tubular necrosis [7]. However, as of yet, treatment effects have not been evaluated and a direct correlation of MR to histopathological changes has not been performed in the context of renal allograft rejection.

The CCL2-specific l-enantiomeric RNA-Spiegelmer mNOX-E36 neutralizes the biological effects of the murine chemokine MCP1 *in vivo* and *in vitro* and ameliorates leukocyte recruitment and inflammatory response in parenchymal interstitial renal disease [8–10]. Spiegelmers are mirror-image oligonucleotides that are able to bind to a pharmacologically relevant target molecule (in this case the chemokine MCP1) similar to an antibody recognizing an antigen. Due to their specific structure, Spiegelmers cannot be recognized by naturally occurring nucleases, resulting in an increased biostability [11]. In a previous study we demonstrated, that mNOX-E36 has a beneficial effect following murine heart transplantation on the acute rejection process in monotherapy with a strong additive effect in combination with a low dose of Ciclosporin A using manual palpation as clinical reference [12], which is obviously not applicable to renal allografts.

The purpose of this study was to investigate the potential of functional MRI-techniques to non-invasively characterize the acute renal allograft rejection process in a murine allogeneic renal transplant model and evaluate the effect of novel pharmacological therapeutics designed to specifically block CCL2.

Materials and Methods

Animals

All procedures involving animals were performed according to the German animal testing Act and approved by the Government of Upper Bavaria (# 55.2-1-54-2531-148-10). C57/Bl6 (H^{2b}) and Balb/c (H^{2b}) mice (Charles River, Sulzfeld, Germany) were maintained in filter topped cages under standard conditions with free access to a standard diet and water. The animals were 7–14 weeks old at the time of transplantation

Orthotopic kidney transplantation

A non-life sustaining transplant technique was performed similar as previously described by Russell et al [13]. Briefly, the left kidney was procured. The renal artery and vein were anastomosed to the aorta and inf. V. cava in end-to-side technique. The time from start of the cold perfusion until reperfusion averaged 59.8 ± 10.8 min. The bladder patch was anastomosed to the recipient's open bladder. The native kidneys of the animals remained in place. Postoperative analgesia was provided with daily buprenorphine s.c.

Experimental groups

Allogeneic and syngeneic transplantations were performed (Balb/c to C57Bl/6 and C57Bl/6 to C57Bl/6) using 37 donor and 37 recipient mice. Taking into account a perioperative failure rate of 30% (death, urinoma, complete renal infarction) a final group size of n = 5 resulted. The CCL2 binding Spiegelmer **mNOX-E36** (5'-GGCGACAUUGGUUGGG CAUGAGGCGAGGC CCUU UGAUGAAUCCGCGGCCA-3') and the inactive control Spiegelmer **revmNOX-E36** (composed of the reverse nucleotide sequence, both conjugated at their 3´ ends with Y-shaped 40 kDa PEG) (5'-ACCGGCGCCUAAGUAGU UUCCCGGAGCGGA GUACGGGUUGGUUACAGCGG-3') are both modified at the 3'-terminus with 40kDa polyethylene glycol and were synthesized at NOXXON Pharma AG (Berlin, Germany)[14]. The animals received either 15.5 mg (based on oligonucleotide weight)/kg body weight mNOX-E36 or non-functional revmNOX-E36 (serving as a control) intraperitoneally every other day. The Spiegelmer was given either as monotherapy or in combination with a low dose of CsA (10 mg/kgBW/d). One further group of mice received CsA (10 mg/kgBW/d) as monotherapy (**Table 1**). Transplanted animals were monitored via MRI on d10 post transplantation and afterwards sacrificed for further *ex vivo* analysis.

MR Imaging

In vivo MR imaging was performed under intraperitoneal Medetomidin-Midazolam-Fentanyl-anesthesia with a clinical 3T-scanner (Magnetom VERIO, Siemens Healthcare Sector, Erlangen, Germany) and a dedicated 8-channel mouse-coil (Rapid Biomedical, Rimpar, Germany) for signal reception. Following morphologic coronal and transversal T1- and T2-weighted sequences, a transversal Echo-Planar-Imaging- sequence (time of

Table 1. Treatment Groups.

Group	Therapy	n =
Sygenic (C57Bl/6 to C57Bl/6)	none	5
Allogeneic (Balb/c to C57Bl/6)	Non-functional revmNOX-E36 (15.5mg/kgBW/q.o.d)	5
Allogeneic (Balb/c to C57Bl/6)	Csa (10mg/kgBW/d)	5
Allogeneic (Balb/c to C57Bl/6)	mNOX-E36 (15.5mg/kgBW/q.o.d)	5
Allogeneic (Balb/c to C57Bl/6)	mNOX-36 + CsA	5

doi:10.1371/journal.pone.0165532.t001

repetition = 2600ms, echo time = 90ms) with ten b-values 0, 10, 30, 50, 80, 120, 200, 400, 600 and 800 s/mm^2 and a resolution of 0.6x0.6x3mm^3 covering the abdomen was acquired for DWI. For DCE-MRI a TWIST-sequence with a spatial resolution of 0.4x0.4x3mm^3 and temporal resolution of 1.5 seconds/slab and total acquisition time of 6 minutes was acquired after tail vein injection of 0.05ml/kg Gadobutrol (Gadovist, Bayer Healthcare Pharmaceuticals, Berlin, Germany) in 100μl saline. The paramagnetic Gadolinium-based contrast agent Gadobutrol causes shortening of the T1-time and thus increased signal in T1-weighted sequences, such as the exploited dynamic sequence. Total acquisition time was approximately 30 minutes. The animals were sacrificed after the MRI-examinations by cervical dislocation and exsanguination, while still under anesthesia. The transplanted kidneys were then harvested for further analysis.

Postprocessing

Postprocessing was performed using the in-house built software PMI 0.4 written in IDL (ITT VIS, Boulder, Colorado, USA). The Apparent Diffusion Coefficient (ADC; mm^2/s*10^{-3}) was derived from whole-kidney ROIs excluding the pelvis defined on parametrical maps calculated from a monoexponential fit of all b-values.

IVIM-metrics for separation of diffusion and pseudodiffusion/perfusion effects were derived as with a voxelwise biexponential analysis [15]. The model for the magnetization M has four parameters: total magnetization M_0, perfusion fraction f_p, pseudo-diffusivity D_p and tissue diffusivity D_t:

$$M = M_0((f_p \exp(-bD_p) + (1 - f_p)\exp(-bD_t)) \quad (1)$$

A *segmented* IVIM-analysis was performed as described previously [16–19] to ensure a more robust analysis compared to an unconstrained fit, albeit at the expense of some accuracy due to the assumptions involved in the separate measurement of D as follows. When the b-value is significantly greater than $1/D_p$ (e.g. for D_p = 10μm^2/ms, 100s/mm^2) the pseudodiffusion term is small, so that Eq (1) can be simplified:

$$M_{high} = M_o((1 - f_p)\exp(-bD_t)) \quad (2)$$

D_t was determined from a monoexponential fit of the asymptotic high b-values range (b> 200 s/mm^2). Its zero intercept $M_0(1\text{-}f_p) = M_{int}$ is used along with the unweighted (b = 0) signal M_0 to determine f_p.

$$f_p = \frac{M_0 - M_{int}}{M_0} \quad (3)$$

Dp—values were calculated from a biexponential fit with constrained D_t and f_p according to Eq (1). Parametric maps of the mean D_t, f_p, and D_p over all directions were generated.

DCE-MRI was analysed based on whole kidney ROIs using model-free deconvolution which is robust and does not impose any constraints on the form of the residue function or the structure of the tissue. It produces a measurement of the impulse response directly from the arterial and tissue tracer concentration. The plasma flow FP (ml/100ml/min) can then be found as the maximum of impulse response. The extracellular volume ECV (ml/100ml) by integration of the impulse response, and the mean transit time (MTT) from the ratio of ECV to FP.

Reverse transcriptase polymerase chain reaction (RT-PCR)

Total RNA was extracted from kidney samples using Trizol (Invitrogen). To determine the mRNA-expression levels 1 μg total RNA was used to perform reverse transcription and

quantitative real time PCR using LightCycler (Roche, Basel, Switzerland) as described previously [20].

Primer sequences were as follows:

Interferon-g: forward 5'-TCAAGTGGCATAG ATGTGGAAGAA-3' and reverse 5'- TGGC TCTGCAGGATTTTCATG-3'.

Tumor necrosis factor-α: forward 5'-CCATTCCTGAGTTCTGCAAG-3', and reverse 5'-GCAAATATAAATAGAGGGGG GC-3'

B-Cell activating factor: forward 5'- TCCAGCAGTTTCACAGCGAT-3', and reverse 5'-TTGACTCCAGCGGTCAACTC-3'

β-Actin: forward 5'-CCCTAAGGCCAACCGTGAAA-3', and reverse 5'-ACGACCAAGG CATACAGGGA-3'.

Normalization was performed against β-Actin as housekeeping gene.

Histology

Harvested allografts were split in half and either paraffin embedded or snap frozen and kept at -80°C. Light microscopy was performed on HE- and PAS-stained whole cross sections of kidney allografts. An experienced blinded nephropathologist (S. M.) evaluated and scored interstitial inflammation, intimal arteritis, tubulitis and glomerulitis as well as periarteritis using a 4-point-score (0–3) and assigned a score according to the Banff criteria [21].

Immunohistochemistry

Immunohistochemistry was performed on 3 μm paraffin embedded cross-sections. Antigen retrieval was performed by Proteinase K (Sigma Aldrich, St. Louis, Missouri) for 20 minutes at 37°C. After blocking with 2.5% goat serum (Vector laboratories, Burlingame, California) the primary antibody (anti–mouse F4/80, 1:100; eBioscience, San Diego, CA) was added for an overnight incubation at 4°C. ImmPRESS HRP kit (Vector laboratories, Burlingame, California) was used for detection. Samples were developed using 3.3'-diaminobenzidine (Sigma Aldrich, St. Louis, Missouri) and nuclear staining was performed using methyl green.

For the analysis five randomly chosen powerfields were analysed per each slide at 20x magnification. Afterwards all slides were analysed using Image J–Image Processing (http://imagej.nih.gov/ij/) adjusting threshold and calculated percents of infiltration area.

Statistical analysis

Statistical analysis was performed with Microsoft Excel 2013 (Microsoft, Redmond, Washington, USA), SPSS 15 (IBM, Armonk, New York USA) and Prism 6.00 software (GraphPad Software, Inc., San Diego, CA). Differences between groups were investigated with unpaired, two-tailed t-tests after testing for normal variance with the Kolmogorov-Smirnov-method. Correlation between the metric MR parameters and metric leukocyte infiltration was determined with Pearsons´s correleation coefficient and correlation to ordinal histopathology with Spearman´s correlation coefficient. Significance was determined at $p<0.05$. We have performed Bonferroni-correction for multiple tests.

Results

Diffusion Weighted Imaging

The ADC (mm^2/s^*10^{-3}) of native kidneys and syngeneic allografts (Fig 1) did not show significant differences (1.29±0.12 vs. 1.17±0.16). Allogeneic controls treated with revmNOX-E36 showed significantly lower ADC (0.63±0.08) than syngeneic allografts ($p<0.001$). Allografts

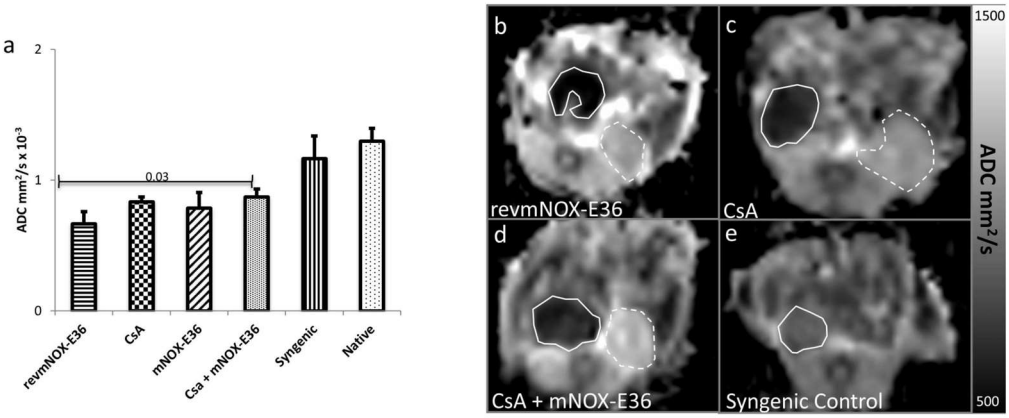

Fig 1. Diffusion Weighted Imaging. (a) Apparent Diffusion Coefficient (ADC): Allograft rejection occurring under revmNOX-E36 shows strong diffusion restriction, i.e. low ADC. Treatment with low dose CsA and mNOX-E36 leads to slight but not significant reduction of the diffusion restriction. Only combined CsA and mNOX lead to a significant increase of ADC, which is still lower than of syngeneic and native kidneys. (b-e) Exemplary parametric ADC-maps (mm^2/s) of orthotopic renal allografts (continuous lines) and native kidneys (broken lines). (b) shows revmNOX-E36, (c) dose CsA, (d) CsA + mNOX-E36, (e) isograft. The images illustrate a strong diffusion restriction occurring without therapy which partially resolves under low dose CsA and CsA + mNOX-E36. There is only slight diffusion restriction for isografts, attributable to ischemia reperfusion.

doi:10.1371/journal.pone.0165532.g001

treated with low dose CsA showed a considerably higher ADC (0.78±0.09) ($p = 0.05$) than revmNOX-E36-controls. Allografts treated with mNOX-E36 only showed a slightly higher ADC (0.83±0.18). The ADC of allografts treated with the combination of CsA and mNOX-E36 were significantly higher (0.90±0.06mm^2/s) than of revmNOX-E36-controls ($p = 0.002$) and slightly higher than of mNOX-E36-monotherapy and still significantly lower than of syngeneic kidneys ($p<0.001$).

IVIM-analysis did not provide additional information (S1 Fig) Tissue diffusivity D_t of allografts was significantly lower than of sygeneic and native kidneys ($p<0.001$), however there was no significant difference between the untreated and treated groups. Perfusion fraction f_p and pseudodiffusion D_p did not show significant differences between all groups.

Dynamic Contrast Enhanced-MRI

Syngeneic allografts and native kidneys (Fig 2) did not show significant perfusion differences (plasma flow (ml/100ml/min): 51.03±12.49 vs. 46.65±11.20) and a significantly higher perfusion than allogeneic allograft controls treated with revmNOX-E36-controls (plasma flow 23.48 ±10.95). Single treatment with mNOX-E36 did not show significant improvement of perfusion (plasma flow 26.60±9.36). Treatment with low dose CsA without or with mNOX-E36 showed an increasing plasma flow (43.43±12.49; 38.75±7.53 ml/100ml/min) which was significantly higher than in untreated allografts ($p<0.01$) and mNOX-E36 monotherapy and not significantly different from native kidneys.

Effect on intragraft proinflammatory cytokines

RT-PCR measurements from the grafts revealed lower levels of B-cell activating Factor (BAFF)-, IFN-γ- and TNF-α- mRNA under the combination therapy compared to

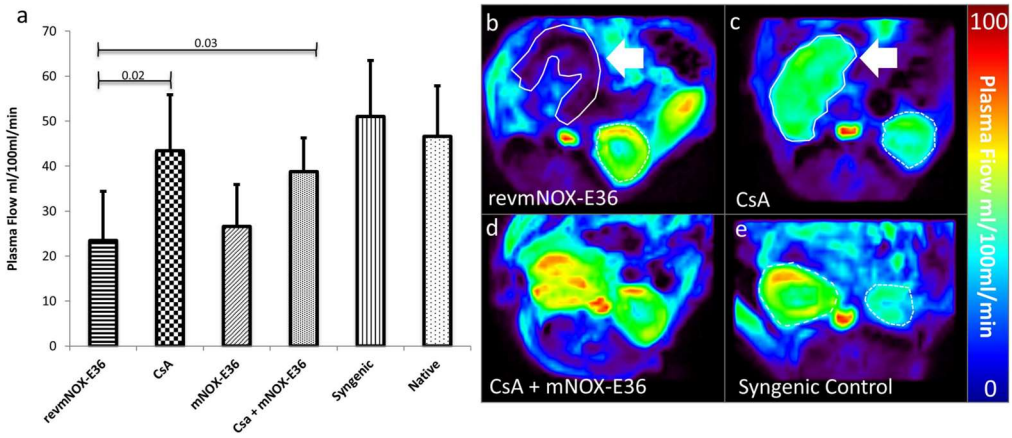

Fig 2. Dynamic Contrast Enhanced–MRI. (a) Plasma flow diagram: Allograft rejection occurring under revmNOX-E36 shows significantly reduced organ perfusion. Treatment with low dose CsA with or without mNOX-E36 leads to significantly increasing organ perfusion, similar to syngeneic and native kidneys. (b-e) Exemplary parametric Plasma flow maps (ml/100ml/min) of orthotopic renal allografts (continuous lines) and native kidneys (broken lines). (b) shows revmNOX-E36, (c) low dose CsA, (d) CsA + mNOX-E36, (e) isograft. The images illustrate a strong reduction of perfusion occurring without therapy. The perfusion deficit resolves already under low dose CsA as well as under CsA + mNOX-E36 with values similar to isografts and native kidneys.

doi:10.1371/journal.pone.0165532.g002

revmNOX-E36 treated controls (BAFF:p<0.0001; IFN-γ:p = 0.0002; TNF-α:p = 0.0005) (Fig 3). Monotherapy with mNOX-E36 resulted in reduced levels of IFN-γ (p = 0.01 vs. control) and TNF-α (p = 0.05 vs. control). Low dose CsA as monotherapy showed similar results with significantly reduced IFN-γ-levels (p = 0.01 vs. control) and BAFF (p = 0.01 vs. control). Of note, combination therapy confirmed an additive effect over monotherapy especially for BAFF

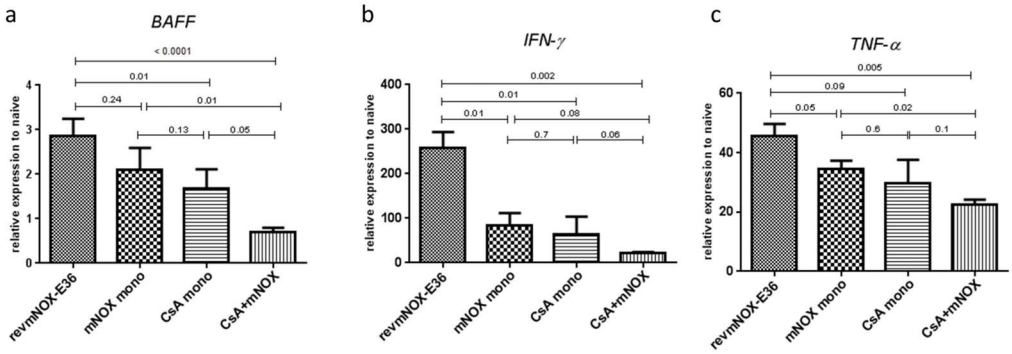

Fig 3. Intragraft pro-inflammatory cytokines. Intragraft mRNA levels of a) B-cell activating Factor (BAFF)-, b) IFN-γ- and c) TNF-α- were significantly reduced under the combination therapy compared to the controls (BAFF: p<0.0001; IFN-γ: p = 0.0002; TNF-α: p = 0.0005). Monotherapy with mNOX-E36 resulted in reduced levels for IFN-γ (p = 0.01 vs. control) and TNF-α (p = 0.05 vs. control) but not for BAFF (p = 0.24). CsA monotherapy significantly reduced IFN-γ- and BAFF-levels (p = 0.01 vs. control) but had less effect on TNF-α (p = 0.09). Combination therapy confirmed again an additive effect over monotherapy.

doi:10.1371/journal.pone.0165532.g003

(combination vs. mNOX-E36, p = 0.01; combination vs. CsA, p = 0.05). IFN-γ-concentrations showed a trend (combination vs. mNOX-E36, p = 0.08; combination vs. CsA, p = 0.06). TNF-α-mRNA levels were significantly reduced under the combination compared to mNOX-E36 (p = 0.02) but not to CsA (p = 0.1).

Histopathology

Ten days after transplantation in accordance to the other results, controls (revmNOX-E36) showed most extensive infarction/necrosis (≥ **80%,** Fig 4). In comparison, under mNOX-E36 treatment only 5–10% of the grafts were affected. No infarction was seen under CsA as monotherapy or in combination with mNOX-36.

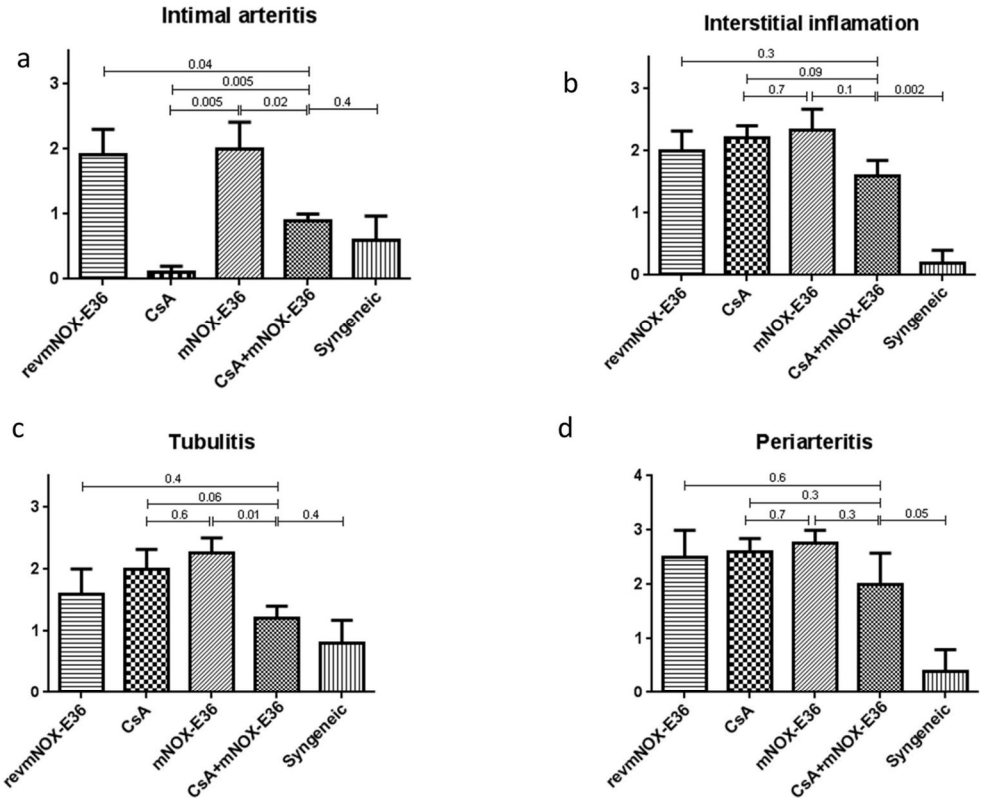

Fig 4. Rejections scores. Rejection scores for a) intimal arteritis, b) interstitial inflammation, c) tubulitis and d) periarteritis were high in all allograft groups. The scores for the combination therapy were significantly reduced only for "intimal arteritis" compared to the controls (p = 0.04). Monotherapy with mNOX-E36 did not show an effect. CsA as monotherapy was significantly reduced only for "intimal arteritis".

doi:10.1371/journal.pone.0165532.g004

Syngeneic control renal transplants had almost no signs of inflammation (intimal arteritis 0.6±0.7; interstitial inflammation 0.2±0.4; tubulitis 0.8±0.7; periarteritis 0.4±0.8) and rejection scores were significantly increased in revmNOX-E36 controls (1.9±0.5; 2.0±0.6; 1.6±0.8; 2.5 ±0.5) and in all treatment groups (interstitial inflammation 1.6 to 2.3; tubulitis 1.2 to 2.3 and periarteritis 2.0 to 2.8) except low dose CsA and combination therapy for intimal arteritis (0.1 ±0.2 and 0.9±0.2). The combination therapy showed reduced scores compared to either low dose CsA or mNOX-E36 for tubulitis (1.2±4 vs. 2.0±0.6 and 2.3±0.0) and a trend for interstitial inflammation (1.6±0.5 vs 2.2 ± 0.4 and 2.3±0.5) and periarteritis (2.0±1.0 vs. 2.6±0.5 and 2.8 ±0.4) (**Figs 4 & 5**). According to the Banff-classification these data showed the following picture: no T-cell mediated rejection and minor capillary/glomerular changes for the syngeneic grafts; moderate-severe T-cell mediated rejection for the combination therapy and CsA as monotherapy; severe T-cell mediated changes for mNOX-E36 and revmNOX-E36 (Table 2).

Immunohistochemistry

Immunohistochemical stainings showed that in revmNOX-E36 treated control renal transplants 22.1±2.3% of the examined area was infiltrated with F4/80+ cells (**Fig 6**). This was significantly increased compared to either low dose CsA (10.8±1.5%, $p<0.0001$) or mNOX-E36 (10.8±1.8%, $p<0.0001$) as monotherapy. Combination therapy of CsA and mNOX-E36 showed an additive effect (5.2±1.2%), with significantly less monocytic infiltration compared to CsA ($p<0.0001$) or mNOX-E36 ($p<0.0001$) monotherapy. Combination therapy reached levels almost comparable to the syngeneic controls (3.4±0.5%).

Correlation between MRI and histologic parameters

There was a significant ($p<0.05$) negative correlation ($r = -0.63$) between perfusion of the transplanted kidney with the degree of the intimal arteritis. Furthermore, we found a significant ($p<0.05$) negative correlation between interstitial inflammation and ADC ($r = -0.73$) and between macrophage infiltration and ADC ($r = -0.81$) (**Fig 7**).

Discussion

Functional MRI may play a complimentary role to histopathology data in diagnosing parenchymal renal disease and the imaging findings of this study were closely correlated to pathophysiology. This is important as invasive biopsy with all its complications such as haemorrhage or infection is currently the only established method to quantitatively assess renal allograft rejection. While several studies have used functional MRI to depict renal pathology in an animal model [22,23], only two studies have assessed renal allograft rejection using functional MRI [24,25]. Several other studies have used functional MRI to identify transplant rejection in heterogeneous patient cohorts [26–30], but up to date no study has utilized functional MRI to directly assess and graduate therapeutic effects in correlation to histology. In the present study, we exploited functional MRI to detect and grade changes under different treatment regimen and to pinpoint these non-invasive imaging findings to a direct histomorphological correlate.

In allogeneic transplanted controls we could demonstrate considerably impaired mobility of water molecules as measured with DWI, potentially related to a) increased cell density due to MCP1-mediated leukocyte recruitment and b) subsequently increased cell volume due to interstitial inflammation as evidenced by histopathology and RT-PCR [31]. Although more refined diffusion techniques such as diffusion tensor imaging and intravoxel incoherent motion imaging assessing tubular integrity and microcirculation have been developed [27,28,32–34], separation of increased cell density and cell volume is not possible with current techniques. Biexponential analysis yielding the microcirculatory diffusion component based on intravoxel

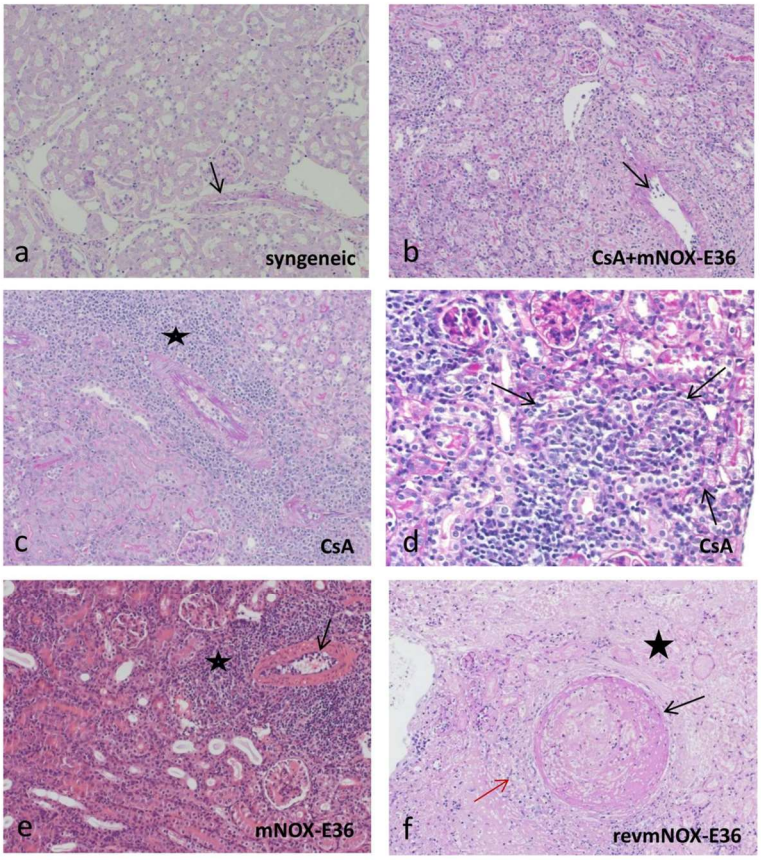

Fig 5. Histopathology of transplant kidneys. magnification 200x; a, b, c, e PAS; d HE a) syngeneic, no therapy (d10 post Tx): no interstitial inflammation, tubulitis or intimal arteritis (arrow); b) allogeneic, CsA+mNOX-E36 (d10 post Tx): mild interstitial inflammation, tubulitis and intimal arteritis (arrow); c) allogeneic, CsA (d10 post Tx): moderate interstitial inflammation and dense perivascular cuff-like lymphocytic inflammation (asterisk), mild intimal arteritis; d) allogeneic, CsA (d10 post Tx): focus of severe tubulitis under CsA monotherapy (arrow); e) allogeneic, mNOX-E36 (d10 post Tx): moderate interstitial inflammation with dense perivascular cuff-like lymphocytic inflammation (asterisk), moderate intimal arteritis (arrow); f) allogeneic, revmNOX-E36 (d10 post Tx): arterial fibrinoid change with medial smooth muscle necrosis (black arrow), mild interstitial inflammation (red arrow). Consecutive ischemic parenchymal necrosis (asterisk).

doi:10.1371/journal.pone.0165532.g005

Table 2. Banff scores.

	Syngeneic	CsA+mNOX-E36	CsA	mNOX-E36	revmNOX-E36
Banff-score	2II, 2II, 2II, 2II, 4IA	3/2II, 4IIA, 4IIA/2II, 4IIA/2II, 4IIA/2II	3/2II, 4IA/2II, 4IA/2II, 4IA/2II, 4IB/2II	4IIB/2II, 4IIB/2II, 4IIB/2II, 4IIB/2II	4IIB/2II, 4IIB/2II, 4IIB/2II, 4III, 4IIB

doi:10.1371/journal.pone.0165532.t002

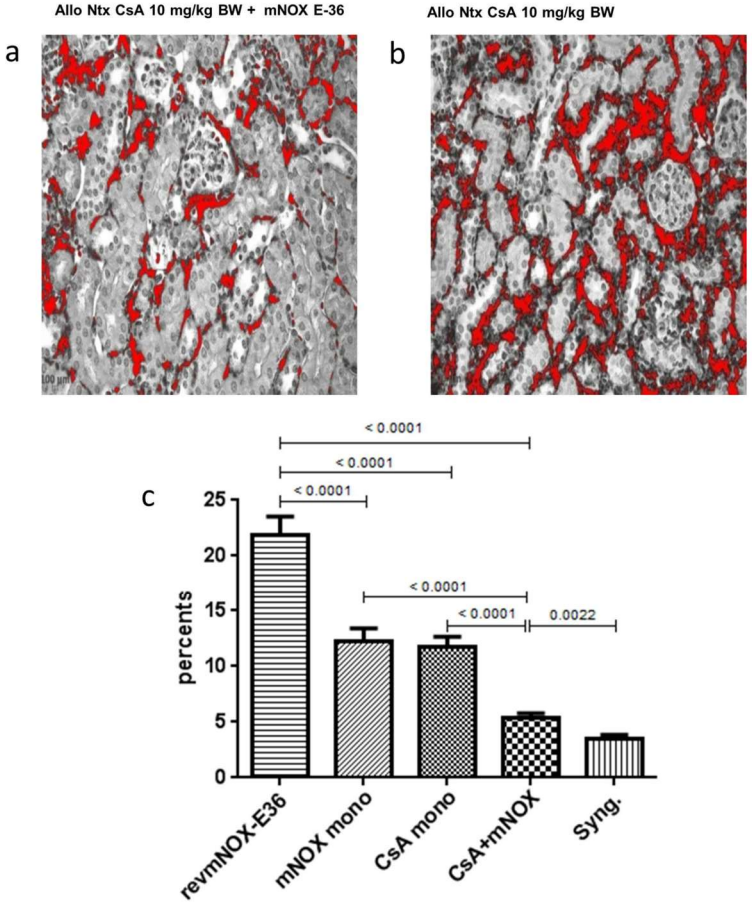

Fig 6. Monocytic infiltrates. Exemplary F4/80+ immunohistochemistry of a specimen treated with (a) low dose CsA + mNOX-E36 or (b) low dose CsA. Under combination therapy considerably less positive F4/80+ cells can be detected. (c) Control grafts (revmNOX-E36) had 22.1±2.3% of the examined area infiltrated with F4/80+ cells. Monotherapy with either mNOX-E36 or low dose CsA showed significant benefits over the controls (10.8±1.8%, $p<0.0001$). Combination therapy showed an additive effect (5.2±1.2%) significantly reduced compared to both monotherapies and ($p<0.0001$) almost reaching levels of syngeneic controls (3.4±0.5%).

doi:10.1371/journal.pone.0165532.g006

incoherent motion was possible with our acquired data, nevertheless the observed findings were inconsistent with a high degree of variation, potentially due to the complex acquisition and postprocessing technique to separate the flow and diffusion compartments. However, in our study the diffusion restriction assessed with the monoexponential analysis was significantly

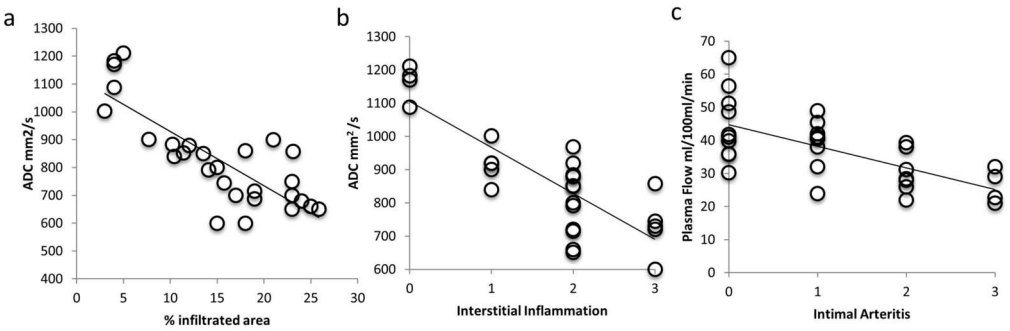

Fig 7. Correlation of functional imaging with histopathology. (a) There was a significant negative correlation between ADC and macrophage infiltration (r = -0.81; p<0.05) determined with immunohistochemistry (F4/80). (b) There was also a significant negative correlation between ADC and interstitial inflammation (r = -0.73; p<0.05) determined with histopatholoy. (c) Furthermore there was a significant negative correlation (r = -0.63; p<0.05) between the reduction of organ perfusion and the degree of intimal arteritis determined with histopathology.

doi:10.1371/journal.pone.0165532.g007

correlated to leukocyte density and interstitial inflammation and decreased with increasing immunosuppression.

DCE-MRI may help further studying the vascular part of allograft rejection by assessing the organ passage of a contrast agent bolus. We found a significant correlation of perfusion parameters with intimal arteritis and corresponding to histopathology low dose CsA with or without mNOX-E36 led to a reduction of microvascular inflammation, a re-established plasma flow and thus restored microcirculation of the transplanted organ.

Principally, in patients DCE-MRI assessed with multi-compartment-models also allows for calculation of split glomerular filtration if a very high temporal resolution is obtained. Our experiments have been performed with a human scanner using dedicated animal equipment, however an already very high temporal resolution of 1.5sec/slab did not allow for a robust calculation of GFR (data not shown), so that only perfusion data based on a deconvolution analysis was available. Examination with dedicated high field small animal scanners may help to further increase the temporal resolution to non-invasively determine glomerular filtration in mice. Overall we could show that combining DWI with DCE-MRI yielded results closely resembling significant parts of histopathology and immunohistochemistry, particularly leukocyte infiltration and vascular inflammation. However, DWI and DCE-MRI are not the only non-invasive techniques allowing assessment of transplant organs. Arterial Spin Labeling MRI, dynamic contrast enhanced ultrasound (CEUS) and CT (DCE-CT)[35] allow for assessment of perfusion similarly to DCE-MRI and have been used in exploratory studies, particularly addressing ischemia-reperfusion damage. However only DWI allows to non-invasively address tissue cellularity, which is linked to leukocyte recruitment and inflammation [6].

The results regarding effectiveness of the novel chemokine-antagonist mNOX-E36 and its histopathological outcome require further addressing. Only few reports investigated the CCL2/CCR2 axis in the context of organ transplantation, showing that inhibition of the chemokine CCL2 or its receptor CCR2 in the lung and islet allograft rejection process significantly prolongs survival [36,37]. Similar results were obtained in a previous laboratory study of our group using a murine heart transplant model with similar therapy regimen [12]. Here, the combination of mNOX-E36/CsA resulted in reduced monocyte infiltration, interstitial tissue damage and

prolonged graft survival. In previously tested parenchymal renal disease models, e.g. diabetes, it was shown that mNOX-E36 effectively blocked macrophage recruitment into the glomerular and interstitial compartments of the kidney [9,10]. Similarly, we found reduced monocytic infiltrates under mNOX-E36 monotherapy. Furthermore, pro-inflammatory cytokines and the ADC as measured by DWI were moderately improved. On the contrary, organ perfusion as measured by DCE-MRI did not recover nor were there improvements using the classical histopathology parameters. When looking at the Banff scores for example, mNOX-E36 was not better than the controls although the extent of infarction/necrosis of the tissue was much less (example Fig 4). Also, the combination therapy failed to show better Banff scores than CsA monotherapy even though the combination led to less interstitial, peritubular and periarterial inflammation. The reason for this was an extraordinary low level of intimal arteritis (v0–0.5) which was even lower than under the combination (v0.5–1). These data were in part confirmed by a non-significant trend towards a better perfusion under CsA mono- vs. combination therapy as measured by DCE-MRI. We lack a good explanation why intimal arteritis was less under CsA monotherapy and can only speculate that the different composition of cellular infiltrates (reduced monocytes under mNOX-E36) or another as of yet unkown cellular/humoral effect is responsible for this.

Importantly, in almost all our experiments a certain additive effect was seen when mNOX-E36 was administered in combination with CsA and that the combination of DCE-MRI and DWI were able to detect these subtle changes.

We furthermore show that histopathology alone with its current scores and classifications lack accuracy. The major weaknesses of the Banff classifications for example are that lesions in the biopsies are empirically derived and thus not specific for any disease entities and their assessment is prone to subjective interpretation and limited reproducibility [38]. These problems have been identified and several Banff working groups are currently focused on a data-driven, evidence-based refinement of the classification [39]. We are convinced that diagnosis of early acute or late ongoing chronic rejection processes should be based on a more multifaceted approach including histology, cellular tests as well as MRI techniques.

Limitations

The measured ADC values were relatively low compared to values found in human studies, which may be attributed to effects of anesthesia and cooling. However this is a systematic error, which will affect all groups alike. Furthermore group size was small with a final group size of n = 5, however one has to take into account, that the orthotopic kidney transplantation model is very demanding with a perioperative failure rate of approximately 30% [13].

Conclusion

In summary, multiparametric functional MRI is suited to detect renal allograft rejection in an experimental murine model and allows to characterize effects of immunosuppressive therapy alleviating acute rejection processes in allogeneic transplantation.

Supporting Information

S1 Fig. Intravoxel Incoherent Motion Analysis. (a): Tissue diffusion D_t: D_t is significantly lower for allografts compared to native and syngenic kidneys, however without significant difference between allograft groups. (b) Pseudodiffusion D_p and (c) perfusion fraction f_p did not show significant differences between all groups.
(TIF)

Author Contributions

Conceptualization: MN AK MK KN JA.

Data curation: MN AK MK MA JA.

Formal analysis: MN AK MK BE SM MNT JA SM.

Funding acquisition: MN JA KN MG JW.

Investigation: MN AK MA JA SM.

Methodology: MN AK MK MA KN JA.

Project administration: MN JA.

Resources: MN JW MG MA JA.

Software: AK MK.

Supervision: MN JW MG KN JA.

Validation: MN AK MG JW KN JA.

Visualization: MK SM JA.

Writing – original draft: MN AK JA KN JW.

Writing – review & editing: MK JA KN JW MG.

References

1. Gondos A, Dohler B, Brenner H, Opelz G (2012) Kidney Graft Survival in Europe and the United States: Strikingly Different Long-term Outcomes. Transplantation.
2. Lamb KE, Lodhi S, Meier-Kriesche HU (2011) Long-term renal allograft survival in the United States: a critical reappraisal. Am J Transplant 11: 450–462. doi: 10.1111/j.1600-6143.2010.03283.x PMID: 20973913
3. Lodhi SA, Lamb KE, Meier-Kriesche HU (2011) Solid organ allograft survival improvement in the United States: the long-term does not mirror the dramatic short-term success. Am J Transplant 11: 1226–1235. doi: 10.1111/j.1600-6143.2011.03539.x PMID: 21564524
4. Hancock WW (2003) Chemokine receptor-dependent alloresponses. Immunol Rev 196: 37–50. PMID: 14617196
5. Franke M, Kramarczyk A, Taylan C, Maintz D, Hoppe B, et al. (2014) Ultrasound-guided percutaneous renal biopsy in 295 children and adolescents: role of ultrasound and analysis of complications. PLoS One 9: e114737. doi: 10.1371/journal.pone.0114737 PMID: 25489731
6. Notohamiprodjo M, Reiser MF, Sourbron SP (2010) Diffusion and perfusion of the kidney. European journal of radiology 76: 337–347. doi: 10.1016/j.ejrad.2010.05.033 PMID: 20580179
7. Eisenberger U, Thoeny HC, Binser T, Gugger M, Frey FJ, et al. (2010) Evaluation of renal allograft function early after transplantation with diffusion-weighted MR imaging. European radiology 20: 1374–1383. doi: 10.1007/s00330-009-1679-9 PMID: 20013274
8. Darisipudi MN, Kulkarni OP, Sayyed SG, Ryu M, Migliorini A, et al. (2011) Dual blockade of the homeostatic chemokine CXCL12 and the proinflammatory chemokine CCL2 has additive protective effects on diabetic kidney disease. The American journal of pathology 179: 116–124. doi: 10.1016/j.ajpath.2011.03.004 PMID: 21703397
9. Kulkarni O, Eulberg D, Selve N, Zollner S, Allam R, et al. (2009) Anti-Ccl2 Spiegelmer permits 75% dose reduction of cyclophosphamide to control diffuse proliferative lupus nephritis and pneumonitis in MRL-Fas(lpr) mice. The Journal of pharmacology and experimental therapeutics 328: 371–377. doi: 10.1124/jpet.108.142711 PMID: 18997060
10. Ninichuk V, Clauss S, Kulkarni O, Schmid H, Segerer S, et al. (2008) Late onset of Ccl2 blockade with the Spiegelmer mNOX-E36-3'PEG prevents glomerulosclerosis and improves glomerular filtration rate in db/db mice. The American journal of pathology 172: 628–637. doi: 10.2353/ajpath.2008.070601 PMID: 18258851

11. Klussmann S, Nolte A, Bald R, Erdmann VA, Furste JP (1996) Mirror-image RNA that binds D-adenosine. Nat Biotechnol 14: 1112–1115. doi: 10.1038/nbt0996-1112 PMID: 9631061
12. Kalnins A, Thomas MN, Andrassy M, Muller S, Wagner A, et al. (2015) Spiegelmer-Inhibition of MCP-1/CCR2—potential as an adjunct immunosuppressive therapy in transplantation. Scand J Immunol.
13. Russell PS, Chase CM, Colvin RB, Plate JM (1978) Kidney transplants in mice. An analysis of the immune status of mice bearing long-term, H-2 incompatible transplants. J Exp Med 147: 1449–1468. PMID: 148488
14. Hoffmann S, Hoos J, Klussmann S, Vonhoff S (2011) RNA aptamers and spiegelmers: synthesis, purification, and post-synthetic PEG conjugation. Curr Protoc Nucleic Acid Chem Chapter 4: Unit 4 46 41–30.
15. Le Bihan D, Breton E, Lallemand D, Grenier P, Cabanis E, et al. (1986) MR imaging of intravoxel incoherent motions: application to diffusion and perfusion in neurologic disorders. Radiology 161: 401–407. doi: 10.1148/radiology.161.2.3763909 PMID: 3763909
16. Callot V, Bennett E, Decking UK, Balaban RS, Wen H (2003) In vivo study of microcirculation in canine myocardium using the IVIM method. Magnetic resonance in medicine: official journal of the Society of Magnetic Resonance in Medicine / Society of Magnetic Resonance in Medicine 50: 531–540.
17. Luciani A, Vignaud A, Cavet M, Nhieu JT, Mallat A, et al. (2008) Liver cirrhosis: intravoxel incoherent motion MR imaging—pilot study. Radiology 249: 891–899. doi: 10.1148/radiol.2493080080 PMID: 19011186
18. Wirestam R, Borg M, Brockstedt S, Lindgren A, Holtas S, et al. (2001) Perfusion-related parameters in intravoxel incoherent motion MR imaging compared with CBV and CBF measured by dynamic susceptibility-contrast MR technique. Acta radiologica 42: 123–128. PMID: 11281143
19. Chandarana H, Lee VS, Hecht E, Taouli B, Sigmund EE (2011) Comparison of biexponential and monoexponential model of diffusion weighted imaging in evaluation of renal lesions: preliminary experience. Investigative radiology 46: 285–291. doi: 10.1097/RLI.0b013e3181ffc485 PMID: 21102345
20. Johnston DR, Sayegh MH, Madsen JC (2002) Overcoming cardiac allograft vasculopathy (CAV) by inducing tolerance. Front Biosci 7: e116–118. PMID: 11991839
21. Racusen LC, Solez K, Colvin RB, Bonsib SM, Castro MC, et al. (1999) The Banff 97 working classification of renal allograft pathology. Kidney Int 55: 713–723. doi: 10.1046/j.1523-1755.1999.00299.x PMID: 9987096
22. Hueper K, Gutberlet M, Rong S, Hartung D, Mengel M, et al. (2014) Acute kidney injury: arterial spin labeling to monitor renal perfusion impairment in mice-comparison with histopathologic results and renal function. Radiology 270: 117–124. doi: 10.1148/radiol.13130367 PMID: 24023073
23. Hueper K, Hartung D, Gutberlet M, Gueler F, Sann H, et al. (2012) Magnetic resonance diffusion tensor imaging for evaluation of histopathological changes in a rat model of diabetic nephropathy. Investigative radiology 47: 430–437. doi: 10.1097/RLI.0b013e31824f272d PMID: 22659594
24. Lee YR, Yang IH, Lee YH, Im SA, Song S, et al. (2005) Cyclosporin A and tacrolimus, but not rapamycin, inhibit MHC-restricted antigen presentation pathways in dendritic cells. Blood 105: 3951–3955. doi: 10.1182/blood-2004-10-3927 PMID: 15657176
25. Hueper K, Hensen B, Gutberlet M, Chen R, Hartung D, et al. (2016) Kidney Transplantation: Multiparametric Functional Magnetic Resonance Imaging for Assessment of Renal Allograft Pathophysiology in Mice. Invest Radiol 51: 58–65. doi: 10.1097/RLI.0000000000000205 PMID: 26371534
26. Heusch P, Wittsack HJ, Blondin D, Ljimani A, Nguyen-Quang M, et al. (2014) Functional evaluation of transplanted kidneys using arterial spin labeling MRI. J Magn Reson Imaging 40: 84–89. doi: 10.1002/jmri.24336 PMID: 24123319
27. Heusch P, Wittsack HJ, Heusner T, Buchbender C, Quang MN, et al. (2013) Correlation of biexponential diffusion parameters with arterial spin-labeling perfusion MRI: results in transplanted kidneys. Invest Radiol 48: 140–144. doi: 10.1097/RLI.0b013e318277bfe3 PMID: 23249648
28. Hueper K, Gutberlet M, Rodt T, Gwinner W, Lehner F, et al. (2011) Diffusion tensor imaging and tractography for assessment of renal allograft dysfunction-initial results. Eur Radiol 21: 2427–2433. doi: 10.1007/s00330-011-2189-0 PMID: 21710264
29. Lanzman RS, Ljimani A, Pentang G, Zgoura P, Zenginli H, et al. (2013) Kidney transplant: functional assessment with diffusion-tensor MR imaging at 3T. Radiology 266: 218–225. doi: 10.1148/radiol.12112522 PMID: 23169797
30. Lanzman RS, Wittsack HJ, Martirosian P, Zgoura P, Bilk P, et al. (2010) Quantification of renal allograft perfusion using arterial spin labeling MRI: initial results. Eur Radiol 20: 1485–1491. doi: 10.1007/s00330-009-1675-0 PMID: 19949799
31. Yang D, Ye Q, Williams DS, Hitchens TK, Ho C (2004) Normal and transplanted rat kidneys: diffusion MR imaging at 7 T. Radiology 231: 702–709. doi: 10.1148/radiol.2313021587 PMID: 15163810

32. Notohamiprodjo M, Glaser C, Herrmann KA, Dietrich O, Attenberger UI, et al. (2008) Diffusion tensor imaging of the kidney with parallel imaging: initial clinical experience. Investigative radiology 43: 677–685. doi: 10.1097/RLI.0b013e31817d14e6 PMID: 18791409

33. Notohamiprodjo M, Chandarana H, Mikheev A, Rusinek H, Grinstead J, et al. (2014) Combined intravoxel incoherent motion and diffusion tensor imaging of renal diffusion and flow anisotropy. Magnetic resonance in medicine: official journal of the Society of Magnetic Resonance in Medicine / Society of Magnetic Resonance in Medicine.

34. Heusch P, Wittsack HJ, Pentang G, Buchbender C, Miese F, et al. (2013) Biexponential analysis of diffusion-weighted imaging: comparison of three different calculation methods in transplanted kidneys. Acta Radiol 54: 1210–1217. doi: 10.1177/0284185113491090 PMID: 23858509

35. Braunagel M, Helck A, Wagner A, Schupp N, Brocker V, et al. (2016) Dynamic Contrast-Enhanced Computed Tomography: A New Diagnostic Tool to Assess Renal Perfusion After Ischemia-Reperfusion Injury in Mice: Correlation of Perfusion Deficit to Histopathologic Damage. Invest Radiol 51: 316–322. doi: 10.1097/RLI.0000000000000245 PMID: 26741893

36. Belperio JA, Keane MP, Burdick MD, Lynch JP 3rd, Xue YY, et al. (2001) Critical role for the chemokine MCP-1/CCR2 in the pathogenesis of bronchiolitis obliterans syndrome. J Clin Invest 108: 547–556. doi: 10.1172/JCI12214 PMID: 11518728

37. Abdi R, Means TK, Ito T, Smith RN, Najafian N, et al. (2004) Differential role of CCR2 in islet and heart allograft rejection: tissue specificity of chemokine/chemokine receptor function in vivo. J Immunol 172: 767–775. PMID: 14707046

38. Furness PN, Taub N, Assmann KJ, Banfi G, Cosyns JP, et al. (2003) International variation in histologic grading is large, and persistent feedback does not improve reproducibility. Am J Surg Pathol 27: 805–810. PMID: 12766585

39. Broecker V, Mengel M (2015) The significance of histological diagnosis in renal allograft biopsies in 2014. Transpl Int 28: 136–145. doi: 10.1111/tri.12446 PMID: 25205033

6. Publikation II

Cathepsin S and Protease-Activated Receptor-2 Drive Alloimmunity and Immune Regulation in Kidney Allograft Rejection

Lei Y*, **Ehle B***, Kumar SV, Müller S, Moll S, Malone AF, Humphreys BD, Andrassy J, Anders HJ. **(*geteilte Erstautorenschaft)**

Cathepsin S and Protease-Activated Receptor-2 Drive Alloimmunity and Immune Regulation in Kidney Allograft Rejection.

Front Cell Dev Biol. 2020 Jun 5;8:398. IF 6.684

frontiers in Cell and Developmental Biology

ORIGINAL RESEARCH
published: 05 June 2020
doi: 10.3389/fcell.2020.00398

Cathepsin S and Protease-Activated Receptor-2 Drive Alloimmunity and Immune Regulation in Kidney Allograft Rejection

Yutian Lei[1]†, Benjamin Ehle[2†], Santhosh V. Kumar[1], Susanne Müller[3], Solange Moll[4], Andrew F. Malone[5], Benjamin D. Humphreys[5,6], Joachim Andrassy[2]* and Hans-Joachim Anders[1]**

[1] Division of Nephrology, Department of Medicine IV, University Hospital, LMU Munich, Munich, Germany, [2] Division for General, Visceral, Transplant, Vascular and Thoracic Surgery, University Hospital, LMU Munich, Munich, Germany, [3] Department of Pathology, University of Munich, Munich, Germany, [4] Institute of Clinical Pathology, University Hospital Geneva, Geneva, Switzerland, [5] Division of Nephrology, Department of Medicine, Washington University in Saint Louis School of Medicine, St. Louis, MO, United States, [6] Department of Developmental Biology, Washington University in Saint Louis School of Medicine, St. Louis, MO, United States

OPEN ACCESS

Edited by:
Songjie Cai,
Brigham and Women's Hospital and Harvard Medical School, United States

Reviewed by:
Robert L. Fairchild,
Cleveland Clinic, United States
Toshiaki Tanaka,
Sapporo Medical University, Japan

***Correspondence:**
Yutian Lei
leiyutian1234@gmail.com
Joachim Andrassy
joachim.andrassy@med.uni-muenchen.de
Hans-Joachim Anders
Hans-Joachim.Anders@med.uni-muenchen.de

†These authors have contributed equally to this work

Specialty section:
This article was submitted to Molecular Medicine, a section of the journal Frontiers in Cell and Developmental Biology

Received: 03 February 2020
Accepted: 29 April 2020
Published: 05 June 2020

Citation:
Lei Y, Ehle B, Kumar SV, Müller S, Moll S, Malone AF, Humphreys BD, Andrassy J and Anders H-J (2020) Cathepsin S and Protease-Activated Receptor-2 Drive Alloimmunity and Immune Regulation in Kidney Allograft Rejection. Front. Cell Dev. Biol. 8:398. doi: 10.3389/fcell.2020.00398

Alloantigen presentation is an essential process in acute allorejection. In this context, we speculated on a pathogenic role of cathepsin S (Cat-S), a cysteine protease known to promote antigenic peptide loading into MHC class II and to activate protease-activated receptor (PAR)-2 on intrarenal microvascular endothelial and tubular epithelial cells. Single-cell RNA sequencing and immunostaining of human kidney allografts confirmed Cat-S expression in intrarenal mononuclear phagocytes. *In vitro*, Cat-S inhibition suppressed CD4 + T cell lymphocyte activation in a mixed lymphocyte assay. *In vivo*, we employed a mouse model of kidney transplantation that showed preemptive Cat-S inhibition significantly protected allografts from tubulitis and intimal arteritis. To determine the contribution of PAR-2 activation, first, Balb/c donor kidneys were transplanted into Balb/c recipient mice without signs of rejection at day 10. In contrast, kidneys from C57BL/6J donor mice revealed severe intimal arteritis, tubulitis, interstitial inflammation, and glomerulitis. Kidneys from *Par2*-deficient C57BL/6J mice revealed partial protection from tubulitis and lower intrarenal expression levels for *Fasl*, *Tnfa*, *Ccl5*, and *Ccr5*. Together, we conclude that Cat-S and PAR-2 contribute to immune dysregulation and kidney allograft rejection, possibly involving Cat-S-mediated activation of PAR-2 on recipient parenchymal cells in the allograft.

Keywords: kidney transplantation, cathepsin S, allorejection, proteinase-activated receptor-2, animal model of transplantation

INTRODUCTION

Among the different forms of renal replacement, therapy kidney transplantation, when available, is the preferred option for most patients with end-stage kidney disease (Wolfe et al., 1999; Robinson et al., 2016). Alloimmunity remains an important factor limiting graft survival, and life-long treatment with relatively non-specific immunosuppressants has remained the standard of care

to date for the vast majority of patients (Durrbach et al., 2010). More selective interference with alloimmunity may broaden the range of options for those patients facing drug toxicity.

Presentation of alloantigen's is a central path mechanism of alloimmunity and involves MHC class II molecules on professional antigen-presenting cells (Borges et al., 2016; Robson et al., 2018). Within antigen-presenting cells, the maturation of MHC class II molecules is tightly regulated, whereby the invariant chain covers the peptide-binding domain up to when peptide loading occurs and the molecule is shuttled to the cell surface (Roche and Frusta, 2015; Robson et al., 2018). Cathepsin (Cat-) S is one of several proteases that chop the invariant chain in a stepwise process (Shi et al., 1999; Roche and Frusta, 2015); hence, Cat-S deficiency or pharmaceutical Cat-S inhibition prevents MHC class II–mediated (auto)antigen presentation (Rise et al., 1996, 1998; Dresden et al., 1999; Saugus et al., 2002; Stickle et al., 2012). Indeed, Cat-S inhibition effectively suppresses the immune dysregulation in numerous experimental autoimmune diseases (Saugus et al., 2002; Baugh et al., 2011; Rupanagudi et al., 2015; Tato et al., 2017).

Beyond its role inside cells, monocytes/macrophages, neutrophils, and endothelial cells secrete Cat-S in the extracellular space where it processes several matrix proteins (Lutgens et al., 2007; Reiser et al., 2010). For example, its elastase activity contributes to vascular wall degeneration in atherosclerosis and aortic aneurysm formation (Shi et al., 2003; Sukhova et al., 2003; Rodgers et al., 2006; Aikawa et al., 2009; Samokhin et al., 2010; Qin et al., 2012; Figueiredo et al., 2015). Indeed, increased serum levels of Cat-S are associated with several cardiovascular risk factors including chronic kidney disease (Jobs et al., 2011, 2013; Lv et al., 2012). As a new finding, we and others recently described that Cat-S activates protease-activated receptor (PAR)-2 on vascular endothelial cells in a thrombin-like manner (Elmariah et al., 2014; Zhao et al., 2014; Kumar et al., 2016). Cat-S-driven PAR-2 activation induced endothelial dysfunction, a central path mechanism in microvascular complications of diabetic mellitus or systemic autoimmunity (Kumar et al., 2016; Tato et al., 2017).

As both mechanisms, MHC class II–mediated antigen presentation and microvascular injury also contribute to immune dysregulation and allograft dysfunction in solid organ transplantation, we hypothesized that interfering with either Cat-S or PAR-2 would attenuate organ injury in a robust model of allograft rejection. To address this concept, we decided for a rigorous mouse model of acute kidney allograft rejection without further immunosuppressive therapy.

MATERIALS AND METHODS

Single-Cell RNA Sequencing of Human Kidney Biopsies

Tissue Processing

The renal biopsy was minced into small pieces with a razor blade and incubated at 37°C in freshly prepared dissociation buffer containing 0.25% trypsin and 40 U/ml DNase I, filtered resuspended in buffer (9% OptiPrep). Nuclei from normal human nephrectomy tissue were isolated with Nuclei EZ Lysis buffer with protease inhibitor and RNase inhibitor. Samples were cut into <2-mm pieces, homogenized, and incubated on ice for 5 min with an additional 2 ml of lysis buffer. The homogenate was filtered, centrifuged, resuspended in suspension Buffer (1 × PBS, 0.07% BSA, 0.1% RNase inhibitor), and counted.

InDrops Single-Cell RNA-Seq

InDrops was performed as described (Klein et al., 2015). In brief, cells were diluted into 60,000 cells/ml in 9% OptiPrep buffer. Single-cell encapsulation was carried out using an inDrops instrument and microfluidic chip manufactured by 1CellBio. In total, 4000 cells were collected. Library preparation was performed according to the protocol provided by the manufacturer. Libraries were sequenced by HiSeq 2500 with a sequencing depth of 50K mapped reads/cell.

10× Single-Nucleus RNA-Seq

RNAs from 6000 single nuclei loaded into one lane of the 10 × Genomics 3-prime V2 platform were encapsulated, barcoded, and reversed transcribed. The library was sequenced in HiSeq 2500 with a sequencing depth of 12.5K mapped reads/cell.

Data Preprocessing

We used the inDrops computational pipeline, dropEst (Klein et al., 2015), to process the single-cell InDrops data. We used STAR to map the high-quality reads to the human genome (GRCh38). We next ran the dropEst program to estimate the accurate molecular counts, which generated a UMI count matrix for each gene in each cell. We used the zUMIs computational pipeline to process the single nuclei data according to protocol (Parekh et al., 2018). In brief, fastq files were filtered for low-quality barcodes and unique molecular identifier (UMIs). Next, cDNA reads were mapped to the reference genome using STAR. Count matrices were generated for exon + intron overlapping reads. These count matrices were used for downstream analysis.

Unsupervised Clustering and Cell Type Identification

UMI count matrices were loaded into the R package Seurat. For normalization, the DGE matrix was scaled by total UMI counts, multiplied by 10,000, and transformed to log space. Only genes found to be expressed in >10 cells were retained. Cells with a relatively high percentage of UMIs mapped to mitochondrial genes (≥0.3) were discarded. Moreover, cells with fewer than 300 or more than 4,000 detected genes were omitted, resulting in 4,487 cells. We also regressed out the variants arising from library size and percentage of mitochondrial genes using the function RegressOut in R package Seurat. The highly variable genes were identified using the function MeanVarPlot with the parameters x.low.cutoff = 0.0125, x.high.cutoff = 6, and y.cutoff = 1, resulting in an output of 2,404 highly variable genes. The expression level of highly variable genes in the cells was scaled and centered along each gene and was conducted to principal component analysis. Based on PCElbowPlot and PCHeatmap Seurat function analysis, we first selected 20 PCs for two-dimensional t-distributed stochastic neighbor embedding (tSNE), implemented by the Seurat software with the default parameters. Based on the

tSNE map, sixteen clusters were identified using the function FindCluster in Seurat with the resolution parameter set to 0.6. We applied the same unsupervised clustering analysis on the single nucleus dataset. After filtering low-quality nuclei, 4,609 nuclei with >400 genes expressed were imported into Seurat for clustering analysis. In total, we identified 13 cell types in the single nucleus dataset, which included macrophages and endothelial cells. Integrated analysis of rejecting and normal human kidney was performed using the Seurat function IntegrateData.

Immunohistochemistry in Human Renal Biopsies

Human renal tissue, fixed in formaldehyde and embedded in paraffin, was selected from the files of the Service of Pathology, University Hospital Geneva: control normal renal tissue was obtained from two patients with nephrectomy performed for neoplasia, involving the possibility of tumor-related immune exhaustion. Five biopsy specimens were obtained from renal transplant patients with acute T cell–mediated rejection. For all biopsy specimens, standard analyses were performed. Each patient gave informed consent before enrollment. The institutional ethical committee board approved the clinical protocol (CEREH number 03-081). The research was performed according to the Helsinki's declaration principles. For immunostaining, serial paraffin sections were stained with the primary antibodies anti-cathepsin S (monoclonal mouse anti-human Cat-S, LSBio, Seattle, WA, United States) and anti-CD68 (DakoCytomation, Glostrup, Denmark) or double stained with anti-cathepsin S and anti-CD68. Counterstaining was performed using Mayer hematoxylin. Negative controls included the absence of the primary antibody (not shown).

Bone Marrow–Derived Dendritic Cell Isolation and Differentiation

For bone marrow–derived dendritic cell (BMDC) preparation, cells were isolated and cultured according to a standard method with minor modifications (Han et al., 1999). Briefly, bone marrow cells were cultured in RPMI 1640 media supplemented with 1% penicillin and streptomycin, 10% of fetal calf serum (S0115, EMD Millipore, United States), 20 ng/ml of mouse recombinant IL-4 and GM-CSF (ImmunoTools, Friesoythe, Germany). At day 8, non-adherent cells were transferred to a fresh plate, primed by 500 μg/ml lipopolysaccharide (LPS, Sigma) for another 24 h, and used for MLR. In BMDC stimulation assays, non-adherent cells were transferred to 12-well plate at 2×10^6/ml at day 8, stimulated with indicated stimuli for 24 h, and analyzed by flow cytometry.

Mixed Lymphocyte Reaction

For *in vitro* assessment of allogenic T-cell activation, mixed lymphocyte reaction (MLR) was set up by incubating T cell–enriched splenocytes together with bone marrow–derived dendritic cells (BMDCs). C57BL/6 (H-2b) and Balb/c (H-2d) mice were used at the age of 7–15 weeks. For T cell preparation, pan T-cells were enriched from splenocytes by a magnetic bead–based negative selection method (Mouse Pan T-cell Isolation Kit II, Miltenyi Biotec, Germany) according to the manufacturer's instruction (purity >90%, data not shown). Purified T cells were labeled with 5 μM carboxyfluorescein succinimidyl ester (CFSE) dye (CellTrace^{TM} CFSE Cell Proliferation Kit, Invitrogen) for 5 min according to the manufacturer's instruction. For proliferation assay, 1.5×10^5 CFSE-labeled T cells and 1×10^5 of primed BMDCs were cocultured in round bottom 96-well plate (Nunc, Germany) for 4 days. Mixed cells were afterward analyzed by flow cytometry to evaluate the proliferation.

Flow Cytometry Analysis

Single-cell suspensions from BMDC stimulation assay or MLR were washed in cold DPBS (PAN Biotech, Germany) twice and suspended in cold FACS buffer (DPBS with 1% BSA and 0.05% sodium azide). Single-cell suspensions were first treated with anti-mouse CD16/32 antibody (BioLegend, United States). Cells from BMDC stimulation assay were stained for anti-mouse CD11c-PE (clone HL3, BioLegend, United States) and anti-mouse MHCII-FITC (clone M5/114.15.2, BioLegend, United States). Cells from MLR were stained for anti-mouse CD8-PE (clone 53-6,7, BioLegend, United States) and then stained for anti-mouse CD4-APC antibody (RM4-4 clone, BioLegend, United States). Samples were analyzed on a flow cytometry analyzer (BD FACSCalibur). For analysis of proliferation, after gating in live/CD4 + CD8- or live/CD4-CD8 +, CFSE histograms were deconvoluted to differentiate each daughter generation from parent cells by software (FlowJo, version 7.6.5) (**Supplementary Figure S1A**). Division index was calculated by the ratio of the total number of divisions over the number of cells at start of culture.

Lactate Dehydrogenase Cytotoxicity Assay

Lactate dehydrogenase (LDH) cytotoxicity assay was set up by mixing 1.5×10^5 of CFSE-stained T cells and 1×10^5 of LPS-primed BMDCs in RPMI 1640 media supplemented with 1% penicillin and streptomycin and 10% of fetal calf serum. Cells were incubated for 4 days. At day 4, cell death was evaluated using LDH cell cytotoxicity assay kit (Roche, Mannheim, Germany) according to the manufacturer's protocol.

Animal Study Design

C57BL/6J (H2b) and Balb/c (H2d) mice were obtained from Charles River (Sulzfeld, Germany) and used at the age of 8–12 weeks. *Par2-/-* mice in the C57BL/6J background were purchased from Jackson Laboratory (Bar Harbor, ME, United States). Offspring were genotyped by polymerase chain reaction (PCR) of genomic DNA derived from tail clippings. Animals were assigned by stratified randomization to different groups co-housed in groups of five in filter top cages with unlimited access to food and water. Cages, nestlets, food, and water were sterilized by autoclaving before use. Humane endpoints were monitored throughout the study. All experiments were conducted according to the European equivalent of the NIH's Guide for the Care and Use of Laboratory Animals and had been approved by the local government authorities.

Kidney transplantations were performed as previously described (Skoskiewicz et al., 1973). Following a midline abdominal incision, the left kidney, aorta, and inferior vena cava of the donor were fully exposed and mobilized. The kidney was procured en bloc including the renal vein; the renal artery, along with a small aortic cuff; and the ureter. The vessels of the graft were anastomosed end-to-side to the recipient's abdominal aorta and inferior vena cava using 10-0 nylon sutures (AROSurgical, Newport Beach, CA, United States). For urinary tract reconstruction, the ureter was directly anastomosed into the bladder using a pull-through (Han et al., 1999). The times of cold and warm ischemia of the graft were maintained at 40 and 30 min, respectively. The native kidneys of the recipient remained untouched as this was a non-life-sustaining approach.

Primary Endpoint: Harvested allografts were split in half and either paraffin embedded or snap frozen and kept at −80°C. Light microscopy was performed on HE- and PAS-stained whole cross sections of kidney allografts. An experienced blinded nephropathologist (S. M.) evaluated and scored for tubulitis, intimal arteritis, interstitial inflammation, and glomerulitis as well as periarteritis using a 4-point-score (0–3) and assigned a score according to the Banff criteria (Haas et al., 2014).

Secondary Endpoints: Real-time reverse transcription-polymerase chain reaction (RT-PCR). Gene expression was assessed by real-time quantitative RT-PCR as described (Lech et al., 2010). In brief, total RNA was isolated using an RNA extraction kit (Life Technologies, Darmstadt, Germany) according to the manufacturer's instructions. After isolation of RNA, cDNA was generated using reverse transcriptase (Superscript II; Invitrogen, Carlsbad, CA, United States). A SYBR Green Dye detection system was used for quantitative real-time PCR on Light Cycler 480 (Roche, Mannheim, Germany) using SYBR Green (SABiosciences) as marker and 18s rRNA as a housekeeping gene. Gene-specific primers blasted with ensemble-BLAST and NCBI primer-BLAST (Metabion, Martinsried, Germany) were used. The following are forward and reverse gene-specific primers, respectively (300 nM; Metabion, Martinsried, Germany): 18s, GCAATTATTCCCCATGAACG and AGG GCCTCACTAAACCATCC; *Ifng*, TGAGCTCATTGAATGCTT GG and ACAGCAAGGCGAAAAAGGAT; *Fasl*, TTAAATGGG CCACACTCCTC and ACTCCGTGAGTTCACCAACC; *Ctss*, GAGTCCCATAGCCAACCACAAG and AAGCGGTGTCTATG ACGACCC; and *Ccl5*, GTGCCCACGTCAAGGAGTAT and CCACTTCTTCTCTGGGTTGG; *Ccr5*, GTCTACTTTCTCTT CTGGACTCC and CCAAGAGTCTCTGTTGCCTGCA; *Foxp3*, CTGGACACCCATTCCAGACT and TTCATGCATCAGCTC TCCAC; *Il2ra*, GCGTTGCTTAGGAAACTCCTGG and GCATA GACTGTGTTGGCTTCTGC, *Cd8b1*, GAATGTGAAGCCAGA GGACAGTG and GGGCAGTTGTAGGAAGGACATC; *Cd4*, GTTCAGGACAGCGACTTCTGGA and GAAGGAGAACTCC GCTGACTCT. Non-template controls consisting of all used reagents were negative for target and housekeeping genes. To reduce the risk of false-positive crossing point, the high-confidence algorithm was used. The melting curve profiles were analyzed for every sample to detect eventual unspecific products or primer dimers.

Histology was a secondary endpoint. Kidneys were fixed in 4% formalin, embedded in paraffin. Immunostaining was performed as described using anti-mouse MHC-II (1:100, clone M5/114.15.2, eBioscience, United States) (Kumar et al., 2016).

Statistical Analysis

Normal data distribution was tested using the Shapiro–Wilk test. Comparisons between two groups were performed with Student's *t*-test or Mann–Whitney *U* test. Comparison of multiple groups was performed with ANOVA or Kruskal–Wallis test; a multiple comparison test was performed with Dunnett or Dunn's correction, respectively. A value of $p < 0.05$ was considered to indicate statistical significance. Data are presented as mean ± SD.

RESULTS

Cathepsin S–Positive Cells Accumulate in Rejecting Human Kidney Allografts

We compared single-cell Cat-S expression (CTSS) in human kidney allograft with mixed rejection and normal human kidney (Wu et al., 2018). Integrated analysis of rejecting and normal human kidney identified 16-cell clusters including all major tubular and immune cell types and endothelial cells (**Figure 1A**). Compared to normal kidney, high expression of CTSS is seen in macrophages and intercalated cells (**Figures 1B** upper, **1C** left). To confirm these data, we performed immunostaining in biopsies from transplanted patients diagnosed with kidney allograft rejection, as well as biopsies from healthy controls. As shown in **Figure 2A**, Cat-S-positive cells were sparse in the interstitium of healthy kidneys and were most likely expressed by CD68 + cells. In contrast, we found numerous CD68/Cat-S double-positive cells accumulating in rejected allografts (**Figure 2B**). Together, Cat-S was strongly expressed inside human kidney allografts.

Cathepsin S Inhibition Suppresses Alloimmune Lymphocyte Proliferation *in vitro*

As Cat-S is a non-redundant component in MHC class II–driven antigen presentation, it should also drive MHC class II–related alloantigen presentation and alloimmunity. We tested this concept by performing mixed lymphocyte assays (**Figure 3A**) and measured CD4 + T lymphocyte division as a readout for alloantigen-specific lymphocyte activation. As shown in **Figure 3B**, Cat-S inhibition did not significantly affect BMDC MHC class II expression. In MLR, however, Cat-S inhibitor–treated groups had less proportion of divided CD4 + T cells (**Figure 3C**). Quantification of the division index also showed that the Cat-S inhibitor suppressed CD4 + T cell and CD8 + T cell division in a dose-dependent manner (**Figures 3D,E**). This effect was independent of cytotoxicity of the Cat-S inhibitor as LDH release was identical in all groups (**Figure 3F**). Thus, we conclude that Cat-S inhibition blocks alloimmune CD4 + and CD8 + T lymphocyte proliferation *in vitro*.

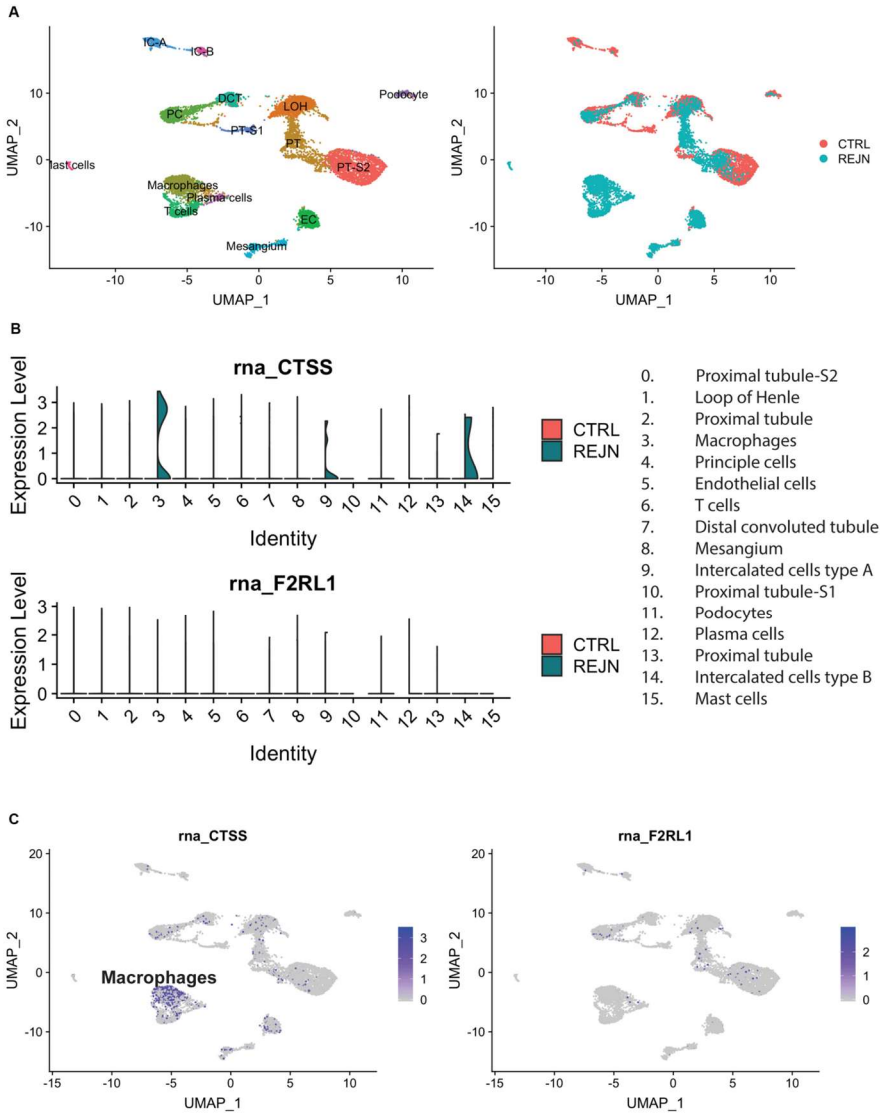

FIGURE 1 | Cat-S and PAR-2 gene expression in healthy and rejected human kidney biopsies by single-cell RNA-seq. **(A)** UMAP plots of combined correlation analysis of a mixed rejection kidney transplant biopsy and a healthy human kidney tissue sample. Left: cell clusters labeled by cell type. Right: clusters labeled according to rejection (blue) or healthy (red) kidney. **(B)** Violin plots of Cat-S (*CTSS*) and PAR-2 (*F2RL1*) gene expression per cell type, in rejection (green) and healthy (red). Upper: *CTSS* expression. Lower: *F2RL1* expression. **(C)** Feature UMAP plots of Cat-S (left) and PAR2 (right) expression. Purple color demotes high gene expression.

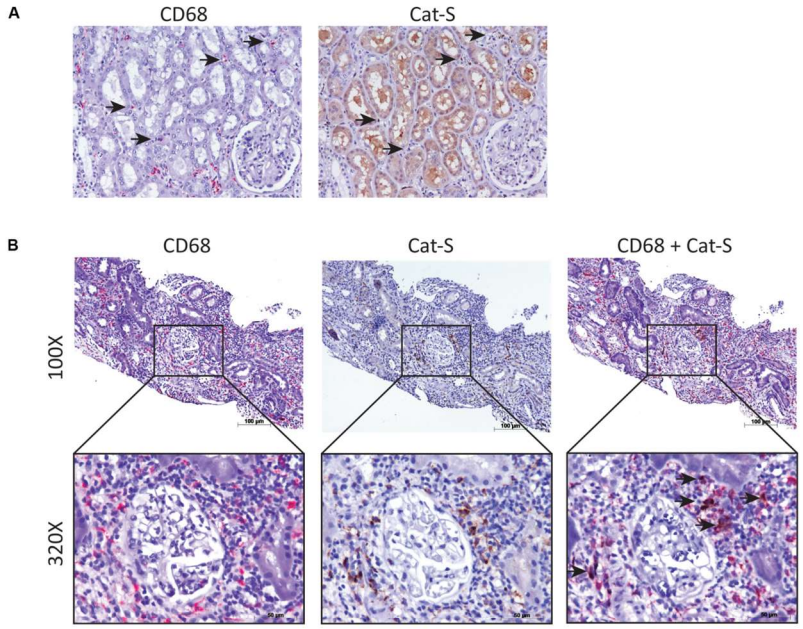

FIGURE 2 | Cat-S expression in kidney biopsies from renal transplant patients with acute T cell–mediated rejection by immunostaining. **(A)** Cat-S and CD68 staining in health human kidney tissue. Consecutive kidney slides were stained for CD68 (left, in red) and Cat-S (right, in brown). CD68-positive cells and Cat-S-positive cells were marked by black arrows. Magnification 200×. **(B)** Cat-S and CD68 staining in rejecting human kidney allografts. CD68 single staining (left), Cat-S single staining (middle), and Cat-S/CD68 double staining (right) was performed on tissues from patients undergoing kidney rejection. Cat-S/CD68 double-positive cells were marked by black arrow.

Preemptive Cathepsin S Inhibition Attenuates Acute Kidney Allograft Rejection

Based on these findings, we tested whether Cat-S inhibition can attenuate kidney allograft rejection *in vivo*. We set up an experimental model based on C57BL/6J (H2b)–recipient mice (**Figure 4A**). We investigated the Cat-S expression in transplanted kidneys. Compared to syngeneic controls, allograft showed numerous Cat-S-positive cells accumulating in the interstitium, especially around vessels (**Figure 4B**). Likewise, Cat-S gene expression was also significantly induced in allograft (**Figure 4C**). Transplanting a kidney from a donor of the same strain showed minimal differences in the histological picture compared to the native kidneys 10 days after the surgery, implying that the transplant procedure *per se* was reliably performed and did not cause tissue damage by ischemia–reperfusion injury (**Figure 4D**). In contrast, kidneys from Balb/c (H2d) donor mice showed signs of severe rejection with tubulitis, glomerulitis, intimal arteritis, and interstitial inflammation (**Figure 4D**). Treating recipient mice with the Cat-S inhibitor RO5461111 completely abrogated tubulitis, intimal arteritis, but not glomerulitis and interstitial inflammation (**Figure 4D**). As a further sign of intrarenal inflammation, quantitative RT-PCR of total kidney RNA revealed increased levels of proinflammatory mediators such as *Ccl5*, *Ccr5*, *Fasl*, and *Ifng* (**Figure 4E**). Cat-S inhibition reduced intrarenal expression levels of above genes. Cat-S inhibition also reduced *Cd4* and *Cd8b1* gene expression (**Figure 4F**). However, it did not affect Foxp3 or Il2ra gene expression (**Supplementary Figure S1B**). The Cat-S inhibitor also did not affect MHC class II expression in graft (**Figure 4G** and **Supplementary Figure S1D**). Cat-S inhibition reduced intrarenal expression levels of the above genes (**Figure 4E**). Taken together, Cat-S inhibition substantially attenuates kidney allograft rejection.

Lack of *Par2* in the Kidney Allograft Attenuates Acute Rejection in Recipient Balb/c Mice

PAR-2 is a G protein receptor and acts as the receptor for many extracellular enzymes, such as Cat-S, trypsin, and tryptase.

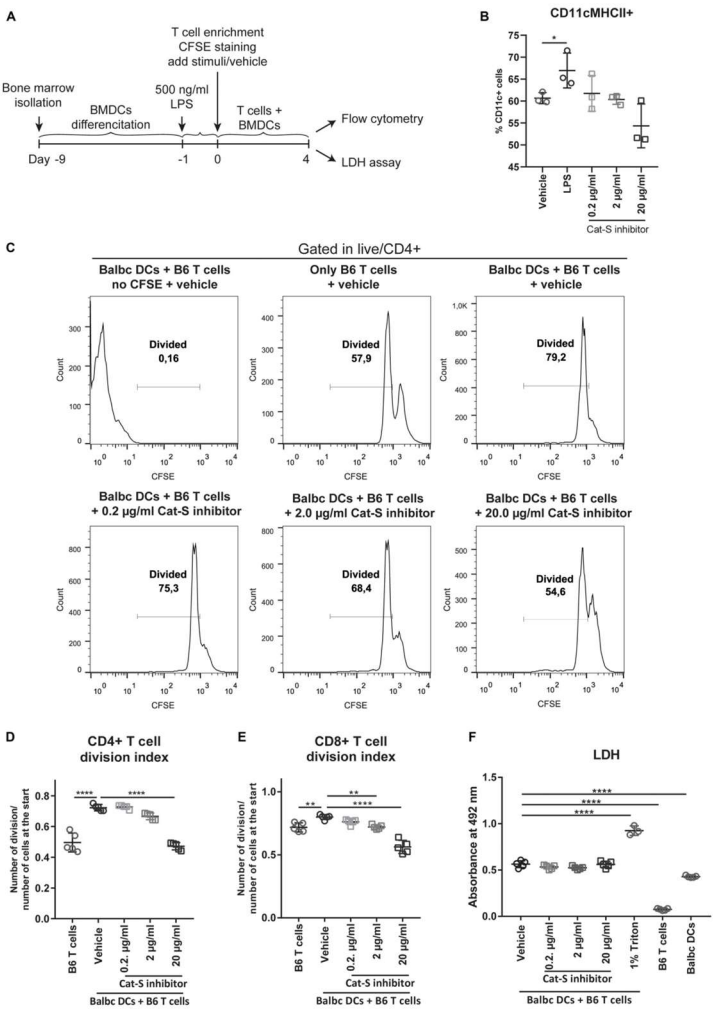

FIGURE 3 | Effect of Cat-S inhibitor on MLR and cytotoxicity. **(A)** Experiment design of mixed lymphocyte reaction for proliferation and LDH assay. LPS-primed BMDCs (Balb/c) and CFSE-stained T cells (C57BL/6J) were used as stimulator and responder, respectively. Mixed cells were cocultured for 4 days and analyzed by flow cytometry or LDH assay. **(B)** BMDC stimulation assays. BMDCs were stimulated with 500 ng/ml LPS, Cat-S inhibitor, or vehicle for 24 h and analyzed for MHC-II expression among CD11c + cells. **(C)** CD4 + T cell proliferation monitored using CFSE labeling. Mixed cells were in the presence of 0.2, 2, 20 μg/ml, or vehicle, and proliferation was analyzed by flow cytometry at 4 days of culture. As controls, mixed cells with no CFSE were treated as the same way as vehicle but without CFSE staining; single T cells were treated with vehicle but without adding BMDCs. After gating in CD4 + cells, divided cells were gated in the histograms of the CFSE channel. A representative experiment from two separate experiments is shown. For each experiment, one mouse was used for BMDC differentiation and two mice were used for T cell isolation. Two or three replications was made from each T cell host for MLR. **(D)** Division index of CD4 + T cells. Based on the deconvoluted histograms of the CFSE channel, the division index was calculated by the ratio of the total number of divisions over the number of cells at start of culture. **(E)** The division index of CD8 + T cells. **(F)** LDH assay for Cat-s inhibitor–treated cells. Supernatant of mixed cell culture was analyzed at day 4 by LDH. $^{*}p < 0.05$, $^{**}p < 0.01$, $^{****}p < 0.0001$.

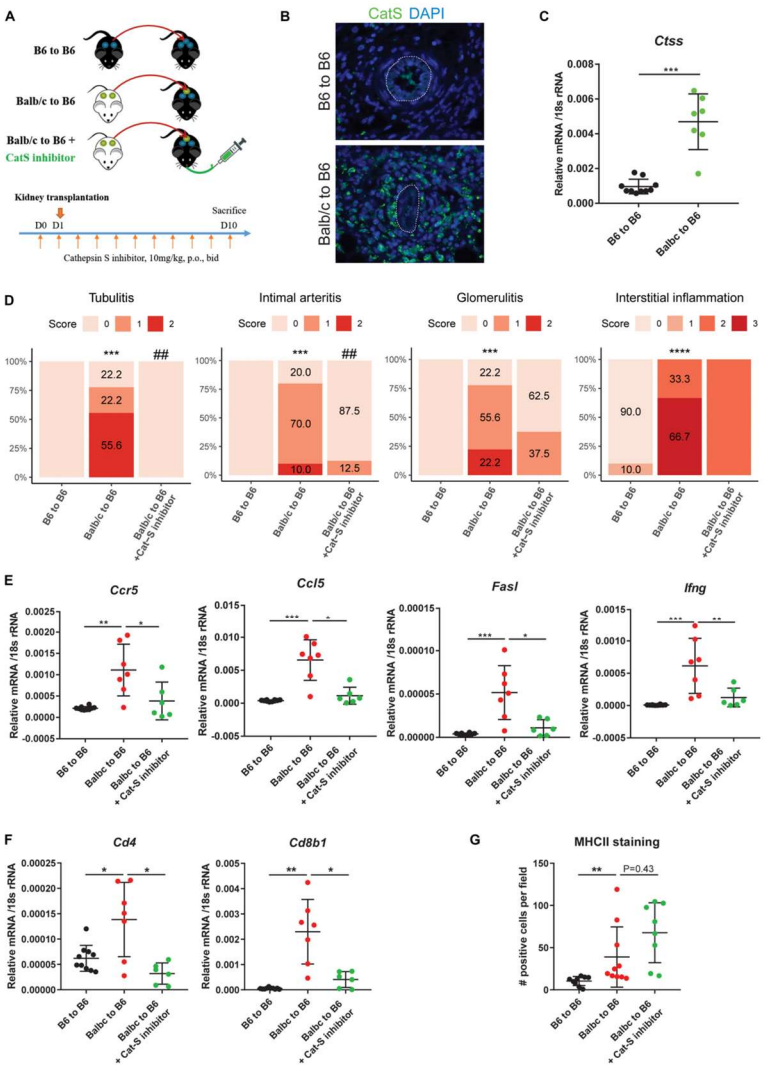

FIGURE 4 | Cathepsin S inhibition attenuated renal allograft rejection *in vivo*. **(A)** Experimental design. Wild-type C57BL/6 kidneys (syngeneic) or wild-type Balb/c kidneys (allogeneic) were transplanted into wild-type C57BL/6 mice. Allogenic recipients were orally administrated with either vehicle or Cat-S inhibitor 10 mg/kg twice daily for a total of 11 days. At day 10 after transplantation, mice were analyzed. **(B)** Cat-S staining in mouse kidney grafts from syngeneic (B6 to B6) and allogeneic group (Balb/c to B6). White dash lines represent for vessels. Magnification 200×. **(C)** *Ctss* mRNA expression in mouse kidney grafts. **(D)** Histological score for mouse kidney grafts. Tubulitis, intimal arteritis, glomerulitis, and interstitial inflammation were quantified by Banff scoring method. $^{***}p < 0.001$ Balb/c to B6 vs. B6 to B6; $^{****}p < 0.0001$ Balb/c to B6 vs. B6 to B6; $^{\#\#}p < 0.01$ Balb/c to B6 vs. Balb/c to B6 + Cat-S inhibitor. $N = 10$ for B6 to B6, $n = 9$–10 for Balb/c to B6, $n = 8$–10 for Balb/c to B6 + Cat-S inhibitor. **(E)** Proinflammation gene expression in mouse kidney grafts by RT-qPCR. **(F)** Cd4 and Cd8b1 gene expression in mouse kidney grafts. **(G)** Quantification of interstitial MHC-II positive cells in mouse kidney graft. $^{*}p < 0.05$; $^{**}p < 0.01$; $^{***}p < 0.001$. B6 represents for C56BL/6J.

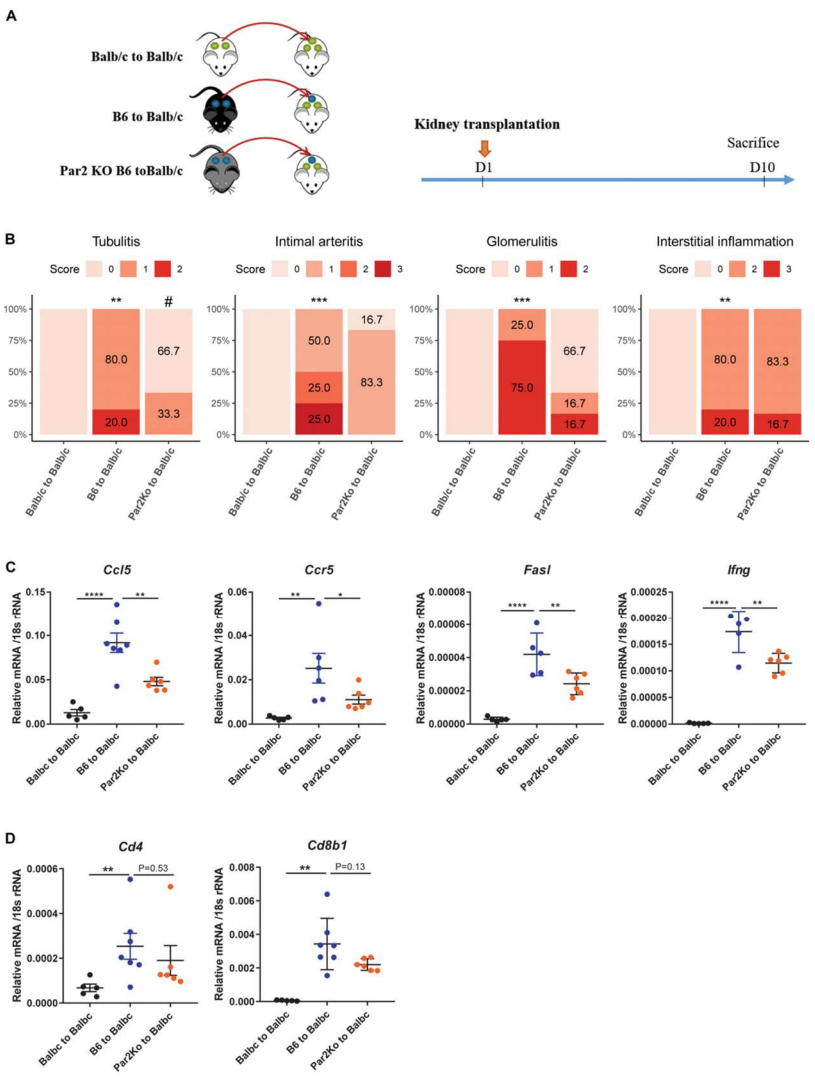

FIGURE 5 | *Par2* deficiency in grafts attenuated renal allograft rejection *in vivo*. **(A)** Experimental design. Wild-type Balb/c kidneys (syngeneic) or wild-type C57BL/6 (allogeneic) were transplanted to wild-type Balb/c mice. *Par2*-deficient kidneys from C67BL/6 background (allogeneic) were transplanted into wild-type Balb/c mice. At day 10 after transplantation, mice were sacrificed for analysis. **(B)** Histological score for mouse kidney grafts. Tubulitis, intimal arteritis, glomerulitis, and interstitial inflammation were quantified by the Banff scoring method. $^{**}p < 0.01$ B6 to Balb/c vs. Balb/c to Balb/c, $^{***}p < 0.001$ B6 to Balb/c vs. Balb/c to Balb/c, $^{\#}p < 0.05$ B6 to Balb/c vs. Par2KO to Balb/c. $N = 4$ for Balb/c to Balb/c, $n = 4$–6 for B6 to Balb/c, $n = 6$ for Par2KO to Balb/c. **(C)** Proinflammation gene expression in mouse kidney grafts by RT-qPCR. **(D)** *Cd4* and *Cd8b1* gene expression in mouse kidney grafts. $^{*}p < 0.05$, $^{**}p < 0.01$, $^{***}p < 0.001$, $^{****}p < 0.0001$. B6 represents for C56BL/6J. Par2KO represent for *Par2* deficiency.

The Cat-S/PAR-2 axis was previously reported to play a role in itch, pain, and diabetic microvasculopathy (Kumar et al., 2016; Zhao et al., 2014; Mihara et al., 2016). Interestingly, using single-cell sequencing data of human kidney allograft rejection, we found F2RL1, the human gene encoding for PAR-2 to be expressed at low levels by several renal parenchymal cell types including endothelial cells and tubular epithelial cells (**Figures 1B** lower, **1C** right). We therefore asked whether PAR-2 also plays a role in this setting. We designed the animal experiment as shown in **Figure 5A**. Compared to kidneys from wild-type B6 donors, kidneys from *Par2*-deficient donor mice showed significantly less tubulitis, non-significant trends toward less glomerulitis, and less intimal arteritis, and no effect on interstitial inflammation (**Figure 5B**). However, *Par2*-deficient allografts also showed reduced expression of the inflammatory genes *Ccl5*, *Ccr5*, *Fasl*, and *Ifng* (**Figure 5C**). In contrast to mice treated with Cat-S inhibitor, Par2-deficient allografts did not show reduced mRNA expression of Cd4 and Cd8b1 (**Figure 5D**) and of *Foxp3* and Il-2ra (**Supplementary Figure S1C**). Together, donor *Par2* deficiency attenuates acute allograft rejection.

DISCUSSION

We had hypothesized that interfering with either Cat-S or PAR-2 would attenuate kidney injury in a robust model of renal allograft rejection. We tested this concept using a pharmacological inhibitor of Cat-S and genetic *Par2* deficiency in different versions of the same kidney transplant model in mice based on the two strains C57Bl/6J (H2b) and Balb/c (H2d). By avoiding additional immunosuppressive therapy, we tested the role of these targets in severe acute rejection. The results confirm the hypothesis and identify Cat-S/PAR-2 as potential molecular targets in the context of solid organ transplantation.

Alloantigen recognition is a central path mechanism of alloimmunity. Both donor- and recipient-derived antigen-presenting cells activate recipient alloreactive T cells to proliferate and circulate, a process leading to alloantigen recognition inside the graft and local alloimmunity, i.e., rejection. These processes involve both MHC class I and II molecules of which peptide loading into MHC class II but not class I molecules is controlled by Cat-S (Rise et al., 1996). In support of this concept, Cat-S inhibition suppressed lymphocyte proliferation in a mixed lymphocyte assay, an accepted *in vitro* model of alloantigen recognition (Ansari and Strom, 2010). Our *in vivo* data further demonstrate that preemptive Cat-S inhibition was sufficient to suppress some aspects of acute renal allograft rejection, namely, tubulitis and arteritis, while, e.g., interstitial inflammation was hardly affected. This may relate to the contribution of MHC class I–mediated alloantigen recognition, and this suggests that monotherapy with a Cat-S inhibitor may be insufficient to control allograft rejection. In this regard, alloimmunity significantly differs from autoimmunity, which can be well controlled by Cat-S inhibitor monotherapy (Rupanagudi et al., 2015; Tato et al., 2017).

However, we and others have previously shown that Cat-S inhibition also prevents Cat-S-mediated activation of PAR-2 on vascular endothelial cells and thereby attenuates endothelial dysfunction–related organ injury (Kumar et al., 2016). In the setting of kidney transplantation, this would imply a potential dual renoprotective effect of Cat-S inhibition, one on alloantigen recognition and one of microvascular injury in the allograft. Indeed, our data show a considerable renoprotective effect of genetic *Par2* deficiency in the allograft. This genetic approach overcomes some of the concerns related to small molecule inhibitors such as exposure, dosing, dosing intervals, and specificity. Nevertheless, we found similar renoprotective effects as compared to the Cat-S inhibitor, indicating that the renoprotective effects of the Cat-S inhibitor largely relate to its activity at PAR-2. However, *Par2* deficiency also abrogates the activity of other serum proteases such as thrombin, which can have similar biological effects (Mihara et al., 2016). Although specific targeting of PAR-2 with drugs would be feasible, in the setting of solid organ transplantation targeting the dual activity of Cat-S appears more promising, potentially in combination with an immunosuppressive drug that also controls MHC class I–mediated alloimmunity.

Obviously, our study presents with some limitations. First, we could not ultimately prove that the *Par2*-dependent effects relate to Cat-S activity. Also, other proteases such as thrombin induce PAR-2 signaling on endothelium and tubular epithelial cells (Vesey et al., 2013; Mihara et al., 2016). Second, because of the robust nature of the acute rejection, it was difficult to quantify immune cell infiltrates and endothelial integrity properly and the life-non-sustaining transplantation technique did not allow testing for renal function. Finally, it would have been desirable to validate the experiments with Cats-deficient mice but such mice fulfilling the microbial requirements of our animal facility could not be obtained.

Together, Cat-S and PAR-2 are potential molecular targets in acute renal allograft rejection. Further studies will evaluate its potential in models that mimic more closely the clinical scenario of acute (and chronic) human allograft rejection.

DATA AVAILABILITY STATEMENT

The datasets generated for this study can be found in the GSE109564 and GSE114156.

ETHICS STATEMENT

The studies involving human participants were reviewed and approved by Committee board University of Geneva (CEREH number 03-081). The patients/participants provided their written informed consent to participate in this study. The animal study was reviewed and approved by Regierung von Oberbayern, Germany.

AUTHOR CONTRIBUTIONS

JA, SK, and H-JA designed the study. BE, SK, and YL performed the mouse study. SuM performed the Banff scoring of mouse kidney. YL and SK performed the *in vitro* study and the mouse sample analysis except Banff scoring. SoM performed the immunostaining of human biopsies. AM and BH performed the single-cell sequencing. YL and H-JA prepared the manuscript. All authors revised and approved the final version of the manuscript.

FUNDING

YL was supported by China Scholarship Council Scholarship. Parts of this project were prepared as a doctoral thesis at the Faculty of Medicine, University of Munich, by BE. This study was supported by the Deutsche Forschungsgemeinschaft (AN372/24-1 to H-JA).

ACKNOWLEDGMENTS

We thank Dan Draganovic, Jana Mandelbaum, Yvonne Minor, Lidia Anguiano Gómez, and Thomas Cagarelli for their expert technical assistance.

SUPPLEMENTARY MATERIAL

The Supplementary Material for this article can be found online at: https://www.frontiersin.org/articles/10.3389/fcell.2020.00398/full#supplementary-material

FIGURE S1 | (A) Gating strategy for proliferation analysis of mixed lymphocyte reaction. **(B)** Foxp3 and Il2ra gene expression in mouse kidney grafts from mice treated with Cat-S inhibitor or vehicle. **(C)** Foxp3 and Il2ra gene expression in mouse kidney grafts from wild type or Par2 deficient mice. **(D)** Representative images of MHC-II staining in mouse kidney grafts treated with Cat-S inhibitor or vehicle. Magnification, 200×.

REFERENCES

Aikawa, E., Aikawa, M., Libby, P., Figueiredo, J. L., Rusanescu, G., Iwamoto, Y., et al. (2009). Arterial and aortic valve calcification abolished by elastolytic cathepsin S deficiency in chronic renal disease. *Circulation* 119, 1785–1794. doi: 10.1161/CIRCULATIONAHA.108.827972

Ansari, M. J., and Strom, T. B. (2010). "Chapter 42 - novel diagnostics in transplantation," in *Chronic Kidney Disease, Dialysis, and Transplantation*, 3rd Edn, eds J. Himmelfarb and M. H. Sayegh (Philadelphia: W.B. Saunders), 609–619. doi: 10.1016/b978-1-4377-0987-2.00042-x

Baugh, M., Black, D., Westwood, P., Kinghorn, E., McGregor, K., Bruin, J., et al. (2011). Therapeutic dosing of an orally active, selective cathepsin S inhibitor suppresses disease in models of autoimmunity. *J. Autoimmun.* 36, 201–209. doi: 10.1016/j.jaut.2011.01.003

Borges, T. J., Murakami, N., and Riella, L. V. (2016). Current status of alloimmunity. *Curr. Opin. Nephrol. Hypertens.* 25, 556–562. doi: 10.1097/mnh.0000000000000267

Dresden, C., Bryant, R. A., Lennon-Dumenil, A. M., Villadangos, J. A., Bryant, P. W., Shi, G. P., et al. (1999). Cathepsin S controls the trafficking and maturation of MHC class II molecules in dendritic cells. *J. Cell Biol.* 147, 775–790. doi: 10.1083/jcb.147.4.775

Durrbach, A., Francois, H., Beaudreuil, S., Jacquet, A., and Charpentier, B. (2010). Advances in immunosuppression for renal transplantation. *Nat. Rev. Nephrol.* 6, 160–167. doi: 10.1038/nrneph.2009.233

Elmariah, S. B., Reddy, V. B., and Lerner, E. A. (2014). Cathepsin S signals via PAR2 and generates a novel tethered ligand receptor agonist. *PloS One* 9:e99702. doi: 10.1371/journal.pone.0099702

Figueiredo, J. L., Aikawa, M., Zheng, C., Aaron, J., Lax, L., Libby, P., et al. (2015). Selective cathepsin S inhibition attenuates atherosclerosis in apolipoprotein E-deficient mice with chronic renal disease. *Am. J. Pathol.* 185, 1156–1166. doi: 10.1016/j.ajpath.2014.11.026

Haas, M., Sis, B., Racusen, L. C., Solez, K., Glotz, D., Colvin, R. B., et al. (2014). Banff 2013 meeting report: inclusion of c4d-negative antibody-mediated rejection and antibody-associated arterial lesions. *Am. J. Transplant.* 14, 272–283. doi: 10.1136/bmjopen-2017-020904

Han, W. R., Murray-Segal, L. J., and Mottram, P. L. (1999). Modified technique for kidney transplantation in mice. *Microsurgery* 19, 272–274. doi: 10.1002/(sici)1098-2752(1999)19:6<272::aid-micr3>3.0.co;2-1

Jobs, E., Ingelsson, E., Riserus, U., Nerpin, E., Jobs, M., Sundstrom, J., et al. (2011). Association between serum cathepsin S and mortality in older adults. *JAMA* 306, 1113–1121. doi: 10.1001/jama.2011.1246

Jobs, E., Riserus, U., Ingelsson, E., Sundstrom, J., Jobs, M., Nerpin, E., et al. (2013). Serum cathepsin S is associated with decreased insulin sensitivity and the development of type 2 diabetes in a community-based cohort of elderly men. *Diabetes Care* 36, 163–165. doi: 10.2337/dc12-0494

Klein, A. M., Mazutis, L., Akartuna, I., Tallapragada, N., Veres, A., Li, V., et al. (2015). Droplet barcoding for single-cell transcriptomics applied to embryonic stem cells. *Cell* 161, 1187–1201. doi: 10.1016/j.cell.2015.04.044

Kumar, S. V., Darisipudi, M. N., Steiger, S., Devarapu, S. K., Tato, M., Kukarni, O. P., et al. (2016). Cleavage of protease-activated receptor-2 on endothelial cells promotes microvascular diabetes complications. *J. Am. Soc. Nephrol.* 27, 1635–1649. doi: 10.1681/ASN.2015020208

Lech, M., vila-Ferrufino, A. A., Skuginna, V., Susanti, H. E., and Anders, H. J. (2010). Quantitative expression of RIG-like helicase, NOD-like receptor and inflammasome-related mRNAs in humans and mice. *Int. Immunol.* 22, 717–728. doi: 10.1093/intimm/dxq058

Lutgens, S. P., Cleutjens, K. B., Daemen, M. J., and Heeneman, S. (2007). Cathepsin cysteine proteases in cardiovascular disease. *FASEB J.* 21, 3029–3041. doi: 10.1096/fj.06-7924com

Lv, B. J., Lindholt, J. S., Cheng, X., Wang, J., and Shi, G. P. (2012). Plasma cathepsin S and cystatin C levels and risk of abdominal aortic aneurysm: a randomized population-based study. *PloS One* 7:e41813. doi: 10.1371/journal.pone.0041813

Mihara, K., Ramachandran, R., Saifeddine, M., Hansen, K. K., Renaux, B., Polley, D., et al. (2016). Thrombin-mediated direct activation of proteinase-activated receptor-2: another target for thrombin signaling. *Mol. Pharmacol.* 89, 606–614. doi: 10.1124/mol.115.102723

Parekh, S., Ziegenhain, C., Vieth, B., Enard, W., and Hellmann, I. (2018). zUMIs - A fast and flexible pipeline to process RNA sequencing data with UMIs. *GigaScience* 7:giy059. doi: 10.1093/gigascience/giy059

Qin, Y., Cao, X., Guo, J., Zhang, Y., Pan, L., Zhang, H., et al. (2012). Deficiency of cathepsin S attenuates angiotensin II-induced abdominal aortic aneurysm formation in apolipoprotein E-deficient mice. *Cardiovasc. Res.* 96, 401–410. doi: 10.1093/cvr/cvs263

Reiser, J., Adair, B., and Reinheckel, T. (2010). Specialized roles for cysteine cathepsins in health and disease. *J. Clin. Investig.* 120, 3421–3431. doi: 10.1172/jci42918

Rise, R. J., Mitchell, R. N., Villadangos, J. A., Shi, G. P., Palmer, J. T., Karp, E. R., et al. (1998). Cathepsin S activity regulates antigen presentation and immunity. *J. Clin. Investig.* 101, 2351–2363. doi: 10.1172/jci1158

Rise, R. J., Wolf, P. R., Bromme, D., Natkin, L. R., Villadangos, J. A., Ploegh, H. L., et al. (1996). Essential role for cathepsin S in MHC class II-associated invariant chain processing and peptide loading. *Immunity* 4, 357–366. doi: 10.1016/s1074-7613(00)80249-6

Robinson, B. M., Akizawa, T., Jager, K. J., Kerr, P. G., Saran, R., and Pisoni, R. L. (2016). Factors affecting outcomes in patients reaching end-stage kidney disease worldwide: differences in access to renal replacement therapy, modality use,

and haemodialysis practices. *Lancet* 388, 294–306. doi: 10.1016/S0140-6736(16)30448-2

Robson, K. J., Ooi, J. D., Holdsworth, S. R., Rossjohn, J., and Kitching, A. R. (2018). HLA and kidney disease: from associations to mechanisms. *Nat. Rev. Nephrol.* 14, 636–655. doi: 10.1038/s41581-018-0057-8

Roche, P. A., and Frusta, K. (2015). The ins and outs of MHC class II-mediated antigen processing and presentation. *Nat. Rev. Immunol.* 15, 203–216. doi: 10.1038/nri3818

Rodgers, K. J., Watkins, D. J., Miller, A. L., Chan, P. Y., Karanam, S., Brissette, W. H., et al. (2006). Destabilizing role of cathepsin S in murine atherosclerotic plaques. *Arterioscler. Thromb. Vasc. Biol.* 26, 851–856. doi: 10.1161/01.atv.0000203526.75772.4b

Rupanagudi, K. V., Kulkarni, O. P., Lichtnekert, J., Darisipudi, M. N., Mulay, S. R., Schott, B., et al. (2015). Cathepsin S inhibition suppresses systemic lupus erythematosus and lupus nephritis because cathepsin S is essential for MHC class II-mediated CD4 T cell and B cell priming. *Ann. Rheum. Dis.* 74, 452–463. doi: 10.1136/annrheumdis-2013-203717

Saugus, K., Ishimaru, N., Yanagi, K., Arakaki, R., Ogawa, K., Saito, I., et al. (2002). Cathepsin S inhibitor prevents autoantigen presentation and autoimmunity. *J. Clin.Investig.* 110, 361–369. doi: 10.1172/jci0214682

Samokhin, A. O., Lythgo, P. A., Gauthier, J. Y., Percival, M. D., and Bromme, D. (2010). Pharmacological inhibition of cathepsin S decreases atherosclerotic lesions in Apoe-/- mice. *J. Cardiovasc. Pharmacol.* 56, 98–105. doi: 10.1097/FJC.0b013e3181e23e10

Shi, G. P., Sukhova, G. K., Kuzuya, M., Ye, Q., Du, J., Zhang, Y., et al. (2003). Deficiency of the cysteine protease cathepsin S impairs microvessel growth. *Circ. Res.* 92, 493–500. doi: 10.1161/01.res.0000060485.20318.96

Shi, G. P., Villadangos, J. A., Dranoff, G., Small, C., Gu, L., Haley, K. J., et al. (1999). Cathepsin S required for normal MHC class II peptide loading and germinal center development. *Immunity* 10, 197–206. doi: 10.1016/s1074-7613(00)80020-5

Skoskiewicz, M., Chase, C., Winn, H. J., and Russell, P. S. (1973). Kidney transplants between mice of graded immunogenetic diversity. *Transplant. Proc.* 5, 721–725.

Stickle, C., Quecke, P., Ruckrich, T., Burster, T., Reich, M., Weber, E., et al. (2012). Cathepsin S dominates autoantigen processing in human thymic dendritic cells. *J. Autoimmun.* 38, 332–343. doi: 10.1016/j.jaut.2012.02.003

Sukhova, G. K., Zhang, Y., Pan, J. H., Wada, Y., Yamamoto, T., Naito, M., et al. (2003). Deficiency of cathepsin S reduces atherosclerosis in LDL receptor-deficient mice. *J. Clin. Investig.* 111, 897–906. doi: 10.1172/jci200314915

Tato, M., Kumar, S. V., Liu, Y., Mulay, S. R., Moll, S., Popper, B., et al. (2017). Cathepsin S inhibition combines control of systemic and peripheral pathomechanisms of autoimmune tissue injury. *Sci. Rep.* 7:2775. doi: 10.1038/s41598-017-01894-y

Vesey, D. A., Suen, J. Y., Seow, V., Lohman, R. J., Liu, L., Gobe, G. C., et al. (2013). PAR2-induced inflammatory responses in human kidney tubular epithelial cells. *Am. J. Physiol. Renal Physiol.* 304, F737–F750. doi: 10.1152/ajprenal.00540.2012

Wolfe, R. A., Ashby, V. B., Milford, E. L., Ojo, A. O., Ettenger, R. E., Agodoa, L. Y., et al. (1999). Comparison of mortality in all patients on dialysis, patients on dialysis awaiting transplantation, and recipients of a first cadaveric transplant. *N. Engl. J. Med.* 341, 1725–1730. doi: 10.1056/nejm199912023412303

Wu, H., Malone, A. F., Donnelly, E. L., Kirita, Y., Uchimura, K., Ramakrishnan, S. M., et al. (2018). Single-cell transcriptomics of a human kidney allograft biopsy specimen defines a diverse inflammatory response. *J. Am. Soc. Nephrol.* 29, 2069–2080. doi: 10.1681/ASN.2018020125

Zhao, P., Lieu, T., Barlow, N., Metcalf, M., Veldhuis, N. A., Jensen, D. D., et al. (2014). Cathepsin S causes inflammatory pain via biased agonism of PAR2 and TRPV4. *J. Biol. Chem.* 289, 27215–27234. doi: 10.1074/jbc.M114.599712

Conflict of Interest: The authors declare that the research was conducted in the absence of any commercial or financial relationships that could be construed as a potential conflict of interest.

7. Literaturverzeichnis

[1] https://dso.de/BerichteTransplantationszentren/Grafiken%20D%202021%20Niere.pdf.

[2] Dutkowski P, de Rougemont O, Clavien PA. Alexis Carrel: Genius, Innovator and Ideologist. Am J Transplant 2008;8:1998-2003.

[3] Starzl T. History of Clinical Transplantation. World J Surg 2000;7:759-782.

[4] Merrill J, Murray J, Harrison J, Guild W. Successful homotransplantation of the human kidney between identical twins. J Am Med Assoc 1956;160:277-282.

[5] Axelrod D, Schnitzler M, Xiao H, Irish W, Tuttle-Newhall E, Chang S, Kasiske B, Alhamad T, K. Lentine. An economic assessment of contemporary kidney transplant Practice. Am J Transplant 2018;18:1168–1176.

[6] Coemans M, Susal C, Döhler B, Anglicheau D, Giral M, Bestard O, Legendre C , Emonds M, Kuypers D, Molenberghs G, Verbeke G, Naesens M. Analyses of the short- and long-term graft survival after kidney transplantation in Europe between 1986 and 2015. Kidney International 2018;94:964–973.

[7] Stegall M, Gaston R, Cosio F, Matas A. Through a glass darkly: seeking clarity in preventing late kidney transplant failure. J Am Soc Nephrol 2015;26:20-29.

[8] Lewis A, Koukoura A, Tsianos G, Gargavanis A, Nielsen A, Vassiliadis E. Organ donation in the US and Europe: The supply vs demand imbalance. Transplant Rev 2021;35:100585.

[9] Callemeyn J, Lamarthee B, Koenig A, Koshy P, Thaunat O, Naesens M. Allorecognition and the spectrum of kidney transplant rejection. Kidney Int 2022;101:692–710.

[10] Langewisch E, Mannon R. Chronic Allograft Injury. Clin J Am Soc Nephrol 2021;16:1723–1729. [11] Hara S. Current pathological perspectives on chronic rejection in renal Allografts. Clin Exp Nephrol 2017;21:943-951.

[12] Mitchell R, Libby P. Vascular Remodeling in Transplant Vasculopathy. Circ Res 2007;100:967- 978.

[13] Cardinal H, Dieudé M, Hébert M. Endothelial Dysfunction in Kidney Transplantation. Front Immunol. 2018;9:1130.

[14] Bouatou Y, Viglietti D, Pievani D, Louis K, Van Huyen J, Rabant M, Aubert O, Taupin J, Glotz D, Legendre C, Loupy A, Lefaucheur C. Response to treatment and long-term outcomes in kidney transplant recipients with acute T cell–mediated rejection. Am J Transplant 2019;19:1972–1988.

[15] Nankivell B, Borrows R, Fung C, O'Connell P, Chapman J, Allen R. Calcineurin Inhibitor Nephrotoxicity: Longitudinal Assessment by Protocol Histology. Transplantation 2004;78:557-565.

[16] Stein J, Nombela-Arrieta C. Chemokine control of lymphocyte trafficking: a general overview. Immunology 2005;116:1–12.

[17] Hancock W. Chemokine receptor-dependent Alloresponses. Immunol Rev 2003;196:37–50.

[18] Deshmane S, Kremlev S, Amini S, Sawaya B. Monocyte Chemoattractant Protein-1 (MCP-1): An Overview. J Interferon Cytokine Res 2009;29:313-326.

[19] Fuentes M, Durham S, Swerdel M, Lewin A, Barton D, Megill J, Bravo R, Lira S. Controlled Recruitment of Monocytes and Macrophages to Specific Organs Through Transgenic Expression of Monocyte Chemoattractant Protein-1. J Immunol 1995;155:5769-5776.

[20] Gelmana A, Okazakia M, Sugimotoa S, Lia W, Kornfelda C, Laia J, Richardsona S, Kreiselb F, Huangc H, Tietjensa J, Zinselmeyer B, Pattersona G, Millerc M, Krupnicka A, Kreisel D. CCR2 Regulates Monocyte Recruitment As Well As CD4+ Th1 Allorecognition After Lung Transplantation. Am J Transplant. 2010;10:1189–1199.

[21] Lee I, Wang L, Wells A, Ye Q, Han R, Dorf M, Kuziel W, Rollins B, Chen L, Hancock W. Blocking the monocyte chemoattractant protein-1/CCR2 chemokine pathway induces permanent survival of islet allografts through a programmed death-1 ligand-1-dependent mechanism. J Immunol 2003;171:6929–6935.

[22] Kalnins A, Thomas M, Andrassy M, Müller S, Wagner A, Pratschke S, Rentsch M, Klussmann S, Kauke T, Angele M, Bazhin A, Fischereder M, Werner J, Guba M, Andrassy J. Spiegelmer Inhibition of MCP-1/CCR2 – Potential as an Adjunct Immunosuppressive Therapy in Transplantation.

Scand J Immunol 2015;82:102–109.

[23] Vater A, Klussmann S. Turning mirror-image oligonucleotides into drugs: the evolution of Spiegelmer therapeutics. Drug Discov Today 2015;20:147-155.

[24] Younga B, Kundua N, Sczepanski J. Mirror-Image Oligonucleotides: History and Emerging

Applications. Chemistry 2019;25:7981–7990.

[25] Notohamiprodjo M, Reiser M, Sourbron S. Diffusion and perfusion of the kidney. Eur J Radiology 2010;76:337–347.

[26] Eisenberger U, Thoeny H, Binser T, Gugger M, Frey F, Boesch C, Vermathen P. Evaluation of renal allograft function early after transplantation with diffusion-weighted MR imaging. Eur Radiol 2010;20: 1374–1383.

[27] Hueper K, Hensen B, Gutberlet M, Chen R, Hartung D, Barrmeyer A, Meier M, Li W, Jang M,

Mengel M, Wacker F, Rong S, Gueler F. Multiparametric Functional Magnetic Resonance Imaging for Assessment of Renal Allograft Pathophysiology in Mice. Invest Radiol 2016;51:58–65.

[28] Quaglia M, Merlotti G, Guglielmetti G, Castellano G, Cantaluppi V. Recent Advances on Biomarkers of Early and Late Kidney Graft Dysfunction. Int J Mol Sci 2020;21:5404.

[29] Morgan T, Chandran S, Burger I, Zhang C, Goldstein R. Complications of Ultrasound-Guided Renal Transplant Biopsies. Am J Transplant 2016;16:1298–1305.

[30] Matar A, Crepeau R, Duran-Struuck R. Non-invasive imaging for the diagnosis of acute rejection in transplantation: The next frontier. Transpl Immunol 2021;68:101431.

[31] Gupta S, Singh R, Dastidar S, Ray A. Cysteine cathepsin S as an immunomodulatory target: present and future trends. Expert Opin. Ther. Targets 2008;12:291-299.

[32] Sena B, Figueiredo J, Aikawa E. Cathepsin S As an Inhibitor of Cardiovascular Inflammation and Calcification in Chronic Kidney Disease. Front Cardiovasc Med 2018;4:88.

[33] Wilkinson R, Williams R, Scott C, Burden R. Cathepsin S: therapeutic, diagnostic, and prognostic potential. Biol Chem 2015;396:867–882.

[34] Riese R, Wolf P, Brömme B, Natkin L, Villadangos J, Ploegh H, Chapman H. Essential Role for Cathepsin S in MHC Class II–Associated Invariant Chain Processing and Peptide Loading. Immunity 1996;4:357–366.

[35] Siu J, Surendrakumar V, Richards J, Pettigrew G. T cell Allorecognition Pathways in Solid Organ Transplantation. 2018;9:2548.

[36] Rock K, Reits E, Neefjes J. Present Yourself! By MHC Class I and MHC Class II Molecules. Trends Immunol 2016;37:724–737.

[37] Alegre M, Lakkis F, Morelli A. Antigen Presentation in Transplantation. Trends Immunol 2016;37:831–843.

[38] Weenink S, Gautam A. Antigen presentation by MHC class II molecules. Immunol Cell Biol 1997;75:69-81.

[39] Roche P, Furuta K. The ins and outs of MHC class II mediated antigen processing and presentation. Nat Rev Immunol 2015;15:203-216.

[40] Saegusa K, Ishimaru N, Yanagi K, Arakaki R, Ogawa K, Saito I, Katunuma N, Hayashi Y. Cathepsin S inhibitor prevents autoantigen presentation and autoimmunity. J Clin Invest 2002;110:361–369.

[41] Riese R, Mitchell R, Villadangos J, Shi G, Palmer J, Karp E, De Sanctis G, Ploegh H, Chapman H. Cathepsin S Activity Regulates Antigen Presentation and Immunity. J Clin Invest 1998;101:2351–2363.

[42] Platta M, Shockey W. Endothelial cells and cathepsins: biochemical and biomechanical regulation. Biochimie 2016;122:314–323.

[43] Vidak E, Javoršek U, Vizovišek M, Turk B. Cysteine Cathepsins and Their Extracellular Roles: Shaping the Microenvironment. Cells 2019;8:264.

[44] Lutgens S, Cleutjens K, Daemen M, Heeneman S. Cathepsin cysteine proteases in cardiovascular disease. FASEB J 2007;21:3029–3041.

[45] Kumar S, Darisipudi M, Steiger S, Devarapu S, Tato M, Kukarni O, Mulay S, Thomasova D, Popper B, Demleitner J, Zuchtriegel G, Reichel C, Cohen C, Lindenmeyer M, Liapis H, Moll S, Reid E, Stitt A, Schott B, Gruner S, Haap W, Ebeling M, Hartmann G, Anders H. Cathepsin S Cleavage of Protease-Activated Receptor-2 on Endothelial Cells Promotes Microvascular Diabetes Complications. J Am Soc Nephrol 2016;27:1635–1649.

[46] Tato M, Kumar S, Liu Y, Mulay S, Moll S, Popper B, Eberhard J, Thomasova D, Rufer A, Gruner S, Haap W, Hartmann G, Anders H. Cathepsin S inhibition combines control of systemic and peripheral pathomechanisms of autoimmune tissue injury. Sci Rep 2017;7:2775.

[47] Tennant G, Wadsworth R, Kennedy S. PAR-2 mediates increased inflammatory cell adhesion and neointima formation following vascular injury in the mouse. Atherosclerosis 2008;198:57–64

[48] Skoskiewicz M, Chase C, Winn HJ Russell P. Kidney transplants between mice of graded immunogenetic diversity. Transplant Proc 1973;5:721-725.

[49] Russell P, Chase C, Colvin R, Plate J. Kidney transplants in mice. An analysis of the immune status of mice bearing long-term, H-2 incompatible transplants. J Exp Med 1978;147:1449-1468.

[50] Wang Z, Wang C, Cunningham E, Allen R, Sharland A, Bishop G. Optimized method for ureteric reconstruction in a mouse kidney transplant model. ANZ J Surg 2014;84:481–485.

[51] Han W, Murray-Segal L, Mottram P. Modified technique for kidney transplantation in mice. Microsurgery 1999;19:272–274.

[52] Loupy A, Mengel M, Haas M. Thirty years of the International Banff Classification for Allograft Pathology: the past, present, and future of kidney transplant diagnostics. Kidney Int 2022;101: 678–691.

[53] Li J, Li C, Zhuang Q, Peng B, Zhu Y, Ye Q, Ming Y. The Evolving Roles of Macrophages in Organ Transplantation. J Immunol Res 2019;2019:5763430.

[54] Belperio J, Ardehali A. Chemokines and Transplant Vasculopathy. Circ Res 2008;103:454-466.

Danksagung

An dieser Stelle möchte ich allen Beteiligten danken, die an der Erstellung der beiden wissenschaftlichen Publikationen mitgewirkt haben, die dieser kumulativen Promotion zu Grunde liegen, insbesondere den beiden Arbeitsgruppenleitern Herrn Professor Hans-Joachim Anders und Herrn Professor Mike Notohamiprodjo.

Ein weiterer Dank gilt Herrn Prof. Dr. med. Jens Werner für die Möglichkeit der Durchführung meiner medizinischen Dissertation an der Klinik für Allgemein-, Viszeral- und Transplantationschirurgie der Ludwig-Maximilians-Universität München.

Mein ganz besonderer Dank gilt meinem Doktorvater Herrn Prof. Dr. med. Joachim Andrassy nicht nur dafür, dass er mich in das faszinierende Gebiet der Transplantationsimmunologie eingeführt hat, sondern auch für das Erlernen der Technik der murinen Herz- und Nierentransplantation. Diese Fertigkeit ist die Grundlage für die wissenschaftlichen Arbeiten dieser Promotion, darüber hinaus jedoch das mentale und handwerkliche Fundament meiner weiteren chirurgischen Ausbildung.

Zutiefst dankbar bin ich meiner Frau Rebecca Ehle für ihre unerschütterliche Unterstützung und immerwährendes Verständnis.

Lebenslauf

Berufserfahrung

JANUAR 2023 BIS HEUTE | ASSISTENZARZT THORAXCHIRURGIE | ASKLEPIOS LUNGENFACHKLINIK GAUTING

Abteilung für Thoraxchirurgie

AUGUST 2022 BIS JANUAR 2023 | ASSISTENZARZT VISZERALCHIRURGIE | KLINIKUM DACHAU

Abteilung für Allgemein-, Viszeral- und Thoraxchirurgie

JULI 2021 BIS JULI 2022 | ASSISTENZARZT THORAXCHIRURGIE | THORAXKLINIK FREIBURG

Abteilung für Thoraxchirurgie

APRIL 2020 BIS JUNI 2021 | ASSISTENZARZT THORAXCHIRURGIE | THORAXKLINIK HEIDELBERG

Abteilung für Thoraxchirurgie

JANUAR 2018 BIS DEZEMBER 2019 | COMMON TRUNK CHIRURGIE | KLINIKUM KAUFBEUREN

Abteilung für Allgemein-, Viszeral-, Thorax- und Gefäßchirurgie

OKTOBER 2008 BIS MÄRZ 2017 | GESUNDHEITS- UND KRANKENPFLEGER IM OP | KLINIKUM GROßHADERN

OP für Allgemein-, Viszeral-, Thorax-, Gefäß- und Transplantationschirurgie

Ausbildung

OKTOBER 2011 BIS DEZEMBER 2017 | STUDIUM DER HUMANMEDIZIN | LUDWIG-MAXIMILIANS-UNIVERSITÄT MÜNCHEN

Gesamtnote 2,66

SEPTEMBER 2005 BIS SEPTEMBER 2008 | AUSBILDUNG ZUM GESUNDHEITS- UND KRANKENPFLEGER | BERUFSFACHSCHULE FÜR KRANKENPFLEGE AM KLINIKUM KAUFBEUREN

Gesamtnote 1,0

JUNI 2005 | ALLGEMEINE HOCHSCHULREIFE | JAKOB-BRUCKER-GYMNASIUM KAUFBEUREN

Gesamtnote 2,6